Proton Stopping in Thin Aluminum Plasmas

B.P. Goel, R.R. Peterson and G.A. Moses

January 1986

FPA-86-1

FUSION POWER ASSOCIATES

2 Professional Drive, Suite 248
Gaithersburg, Maryland 20879
(301) 258-0545

1500 Engineering Drive
Madison, Wisconsin 53706
(608) 263-2308

PROTON STOPPING IN THIN ALUMINUM PLASMAS

B.P. Goel

G.A. Moses

R.R. Peterson

Fusion Power Associates
6519 Grand Teton Plaza
Madison, WI 53719

January 1986

FPA-86-1

I. INTRODUCTION

Ion beam-target interaction is a key issue for the successful design of inertial confinement fusion (ICF) targets. The particle range must be known to an accuracy of better than 10% to optimize target designs. Too short a range will cause a larger amount of material to implode thereby reducing the implosion velocity. On the other hand if the range is larger than that computed by target design codes the beam will penetrate deeper into the target, reducing the amount of pusher and preheating the fuel. In principle, low intensity beams, as used in nuclear physics research, can be used to measure stopping power. The matter in this case has to be heated by an external source. This, however, requires confining the plasma at very high temperature, with well defined thermodynamical conditions for a sufficiently long time. One method of creating such a plasma is the use of an intense laser, but the physics of energy deposition is not uniform and will greatly complicate the analysis of results. Another way of creating the plasma, the method proposed in this paper, is to use intense ion beams. In this scheme, the same ion beam would make the plasma, through vaporization of a target, deposit the energy in the plasma to be measured. In this case plasma properties such as temperature, density, degree of ionization, etc., change during the course of the experiment. These in turn have a marked influence on the energy deposition of the incoming particle beam. Analytical models have been formulated for idealized cases[1-5] of this plasma behavior. These formulae, in addition to other simplifications, do not take the change in stopping power with material properties into account. In real experiments[6,7] the situation is far more complicated than can be formulated with simple analytical formulae. Not only does the stopping power of the beam change with material properties but

also the beam characteristics, such as its energy and power, change with time in a way that precludes simple formulation. To further complicate the situation only a fraction of the particle beam consists of the required species, e.g., proton impurities are present in non-negligible amounts. The non-normal incidence of the beam on the expanding target must also be taken into account. In general, a complete numerical simulation of hydro and thermodynamic effects together with beam stopping calculations is required to analyze dE/dx experiments.

At the Kernforschungszentrum Karlsruhe a pulse power machine (KALIF) has been installed. Using a 6 cm pinch reflex diode, a 1.5 MeV proton beam has been focused to 0.3 TW/cm^2 on a target.[8] A peak power of 0.7 TW was observed. Higher power densities may be obtained in the near future by optimizing the diodes and improving the machine performance. The ion beam pulse is about 60 ns long (FWHM). With these characteristics KALIF can serve as a suitable tool to measure energy deposition of light ions in the temperature range of a few 10's of eV. In this paper we examine the range in which meaningful dE/dx measurements can be performed on KALIF with its present operating characteristics. We first review our hydrodynamics and beam plasma coupling models in Sections II and III. In Section IV we compare the results of our codes with recently published results from NRL.[9] Since the ion coupling model and the hydrodynamics treatment are different in the NRL calculations from our own codes, this comparison serves as a good check on the soundness of our results. In Section V we examine the range in which meaningful dE/dx measurements can be performed on the KALIF facility. These calculations are performed for a 7.5 μm thick Al target. In Section VI conclusions are drawn from this work.

II. HYDRODYNAMICS MODEL

Calculations are performed using two different Lagrangian hydrodynamics codes MEDUSA-KA[10-12] and PHD-IV.[13,14] Details of these codes have been reported previously. In the following only a brief summary of the main features relevant to the present work is given.

Both of the programs are one-dimensional, Lagrangian hydrodynamics codes written initially to study laser driven ICF implosions. The basic equations solved are the one fluid-two temperature equations of plasma hydrodynamics:

$$\frac{\partial U}{\partial t} = \frac{1}{\rho} \nabla P \tag{1}$$

$$\rho C_{ve} \frac{\partial T_e}{\partial t} = \nabla \cdot k_e \nabla T_e - P_e (\nabla \cdot U) - \omega_{ei} (T_e - T_i) + S_e \tag{2}$$

$$\rho C_{vi} \frac{\partial T_i}{\partial t} = \nabla \cdot k_i \nabla T_i - P_i (\nabla \cdot U) + \omega_{ei} (T_e - T_i) + S_i \tag{3}$$

U is the fluid velocity, ρ is the mass density, $P = P_e + P_i$ is the pressure, C_v is the specific heat, T is the temperature, subscript i denotes ion and e denotes electrons. The conductivity coefficients $k_{e,i}$ and electron-ion equilibration coefficient ω_{ei} are taken from Spitzer.[15] The source terms S_e and S_i are, in the present context, the energy deposited by the ion beam to the plasma. Ions and electrons can have different temperatures but both the fluids travel with the same speed so that no charge separation takes place and the generation of electric fields is avoided. PHD-IV can treat radiation as a third temperature or can use a multigroup transport of radiation.[14] The radiation transport coefficients are taken from the Los Alamos opacity library.[16]

The two populations (electrons and ions) are governed by their own pressures. For ions it is deemed sufficient to use an ideal gas equation of state. Electrons, however, require a more complex treatment. The code PHD-IV reads the equation of state data from the SESAME library.[17] In MEDUSA-KA an analytical equation of state is used. This has the form

$$P_e(\rho,T) = P_c(\rho) + P_B(\rho,T) + P_f(\rho,T)$$

P_c denotes cold or zero temperature curve, $P_B(\rho,T)$ and $P_f(\rho,T)$ are the components due bound and free electrons in the plasma. Different options to calculate P_e are available.[17] For the present calculations the so-called corrected Thomas-Fermi equation of state is used.

The correction to the Thomas-Fermi equation of state is obtained by an expansion of the Hartree-Fock equation in series of progressively higher order quantum terms. Retaining the first order quantum term yields the corrected Thomas-Fermi equation of state.[11,19] The correction term has the same form as obtained by including the exchange forces. Thus, first order quantum effects and exchange forces can be accounted for by using the same term multiplying it by an appropriate numerical factor. The zero temperature part of this term can be separated from the temperature dependent part. For the sake of simplicity MEDUSA-KA uses only the zero temperature part of the correction term.[18]

In Fig. 1, plasma pressure for aluminum as calculated in MEDUSA-KA is compared with that used in PHD-IV, which uses the SESAME equation-of-state library. One sees that there is very good agreement between the calculated MEDUSA-KA values and the tabulated PHD-IV values.

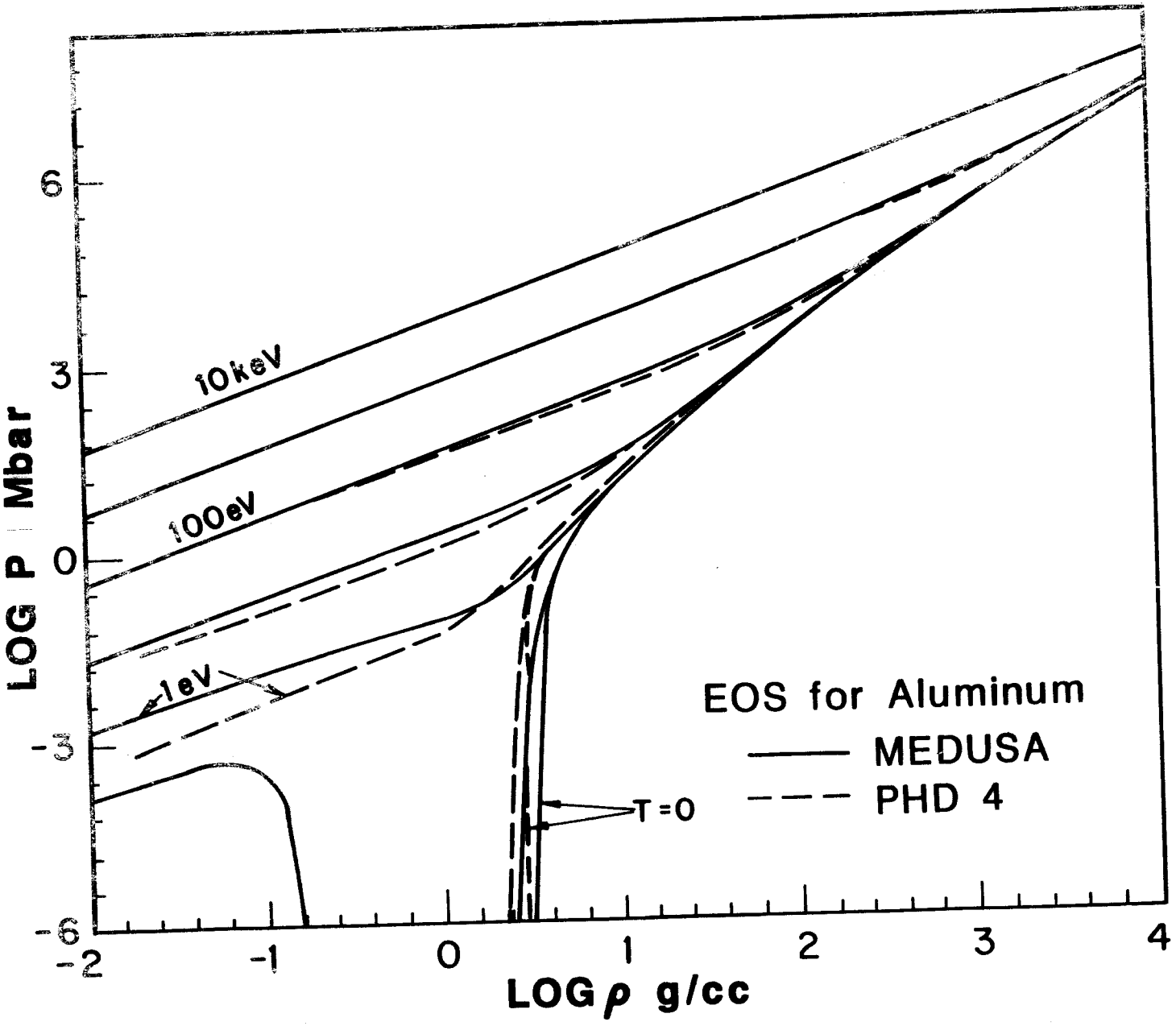

Fig. 1. Plasma Pressure versus Density for Aluminum for Various Temperatures. Values calculated by MEDUSA-KA are compared with those from PHD-IV, where the SESAME equation-of-state tables are used.

III. BEAM TARGET COUPLING MODEL

The source terms in Eqs. (2) and (3) are determined by the amount of energy deposited in the plasma by the ion beam interaction. They depend on the beam energy and on the temperature and density of the target. There is a great deal of information available on the ion stopping in cold material.[20] Less is known about the stopping of charged particles in hot dense media. Only recently have experiments been performed to measure the stopping power of protons in hot plasma.[6,7] Enhancement of the stopping power in hot plasma has been observed.

A fair amount of theoretical work has been done to calculate stopping of charged particles in hot plasma.[16-22] All calculations of stopping power treat bound and free electrons separately. Others have suggested that this distinction may not be a valid assumption in dense plasmas.[28]

In a general form the stopping power can be written as:

$$\frac{dE}{dx} = \left[\frac{dE}{dx}\right]_{bound} + \left[\frac{dE}{dx}\right]_{free} + \left[\frac{dE}{dx}\right]_{ions} .$$

The ion stopping is important only at low energies or in low atomic weight materials. The calculation for the bound electron stopping power is done using Bethe's theory.[29] Bethe's equation can be written as

$$\frac{dE}{dx} = \frac{4\pi Z_B^2 Ze^4 N}{m_e v^2}\left[\ln\frac{2m_e v^2}{I} - \beta^2 - \sum_i \frac{C_i}{Z} - \frac{\delta}{2}\right] .$$

Z_B is the charge number, v the velocity of the beam particle, $\beta = v/c$; Z and N are the charge number and the number density of the field particles. C_i and δ are the correction terms due to shell effects and polarization. The basic

parameter in Eq. (4) is the average ionization potential I. Different approaches of calculating the ion stopping differ in the way I is calculated. At KfK, the code GORGON[30] is used. This code is based on the work of Nardi and Zinamon.[21] A semi-classical procedure based on Bohr's model is used to calculate I. Shell effects are included by excluding from the integral atomic electrons moving faster than the beam ions. However, the calculation is time consuming and not suitable for incorporation in a hydrodynamics code. The alternate procedure is to obtain values of I from appropriate calculations and use an analytical fit to these I values in the dE/dx calculation. We use the analytical fit of Mehlhorn et al.[25] to the data of McGuire et al.[26] Figure 2 shows the result of this latter approach (marked EDEPOS) to the GORGON results. It is seen that the agreement between the two approaches is reasonably good except at low energies. At these low energies, however, uncertainty even in the cold data is large.[20]

IV. COMPARISON WITH PUBLISHED RESULTS

In this section the results of our calculations are compared with a recent publication by Rogerson et al. (NRL).[9] The problem analyzed is a 16 TW/cm^2, 1 MeV proton beam incident on a 15 μm thick aluminum slab for 10 ns, shown in Fig. 3. Their method of solution is somewhat different than our approach. They use a sliding zone Eulerian hydrodynamics code in contrast to our Lagrangian approach. They also use a collisional radiative equilibrium treatment of the ionization balance.[31] However, in their calculation an average charge value is used. They use a modified ideal gas equation of state, whereas in our codes a more realistic equation of state is used. The energy coupling is also somewhat different between the two approaches. Figure 4 shows the energy deposited by 1 MeV protons in each of the 20 equal mass

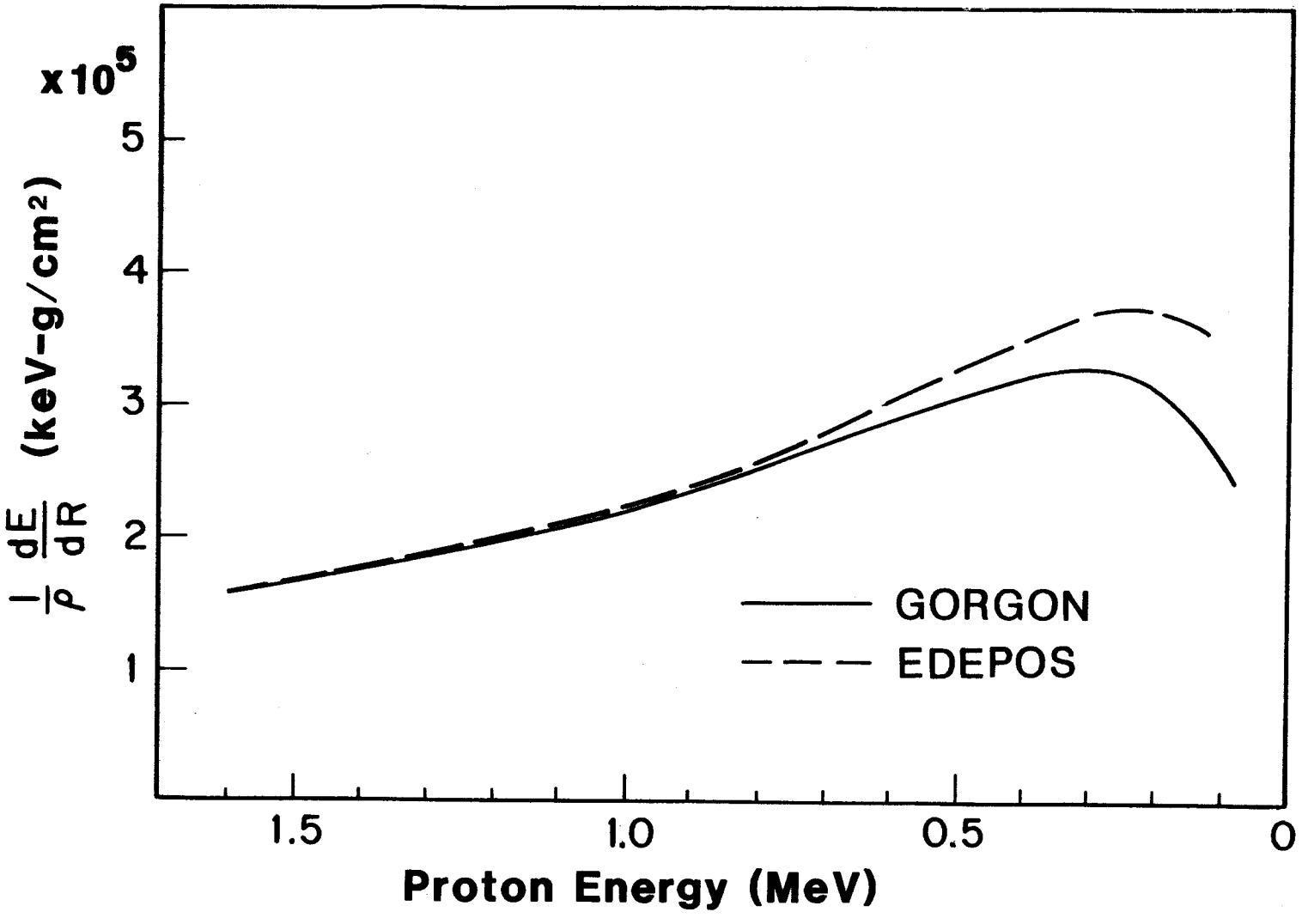

Fig. 2. Proton Stopping Powers in Aluminum at 100 eV versus Proton Energy. Values calculated by the GORGON code are compared with those from the EDEPOS subroutine used in both MEDUSA-KA and PHD-IV.

N R L – Problem

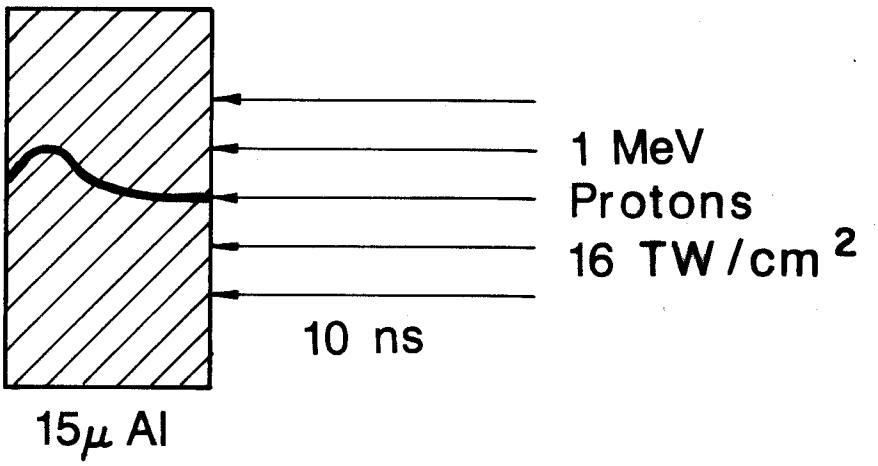

J.E. Rogerson, R.W. Clark and J. Davis; Phys. Rev. A 31 (1985) 3323

Fig. 3. Schematic Picture of the "NRL Problem." 16 TW/cm^2 of 1 MeV protons are incident on a 15 μm thick aluminum target in a 10 ns pulse.

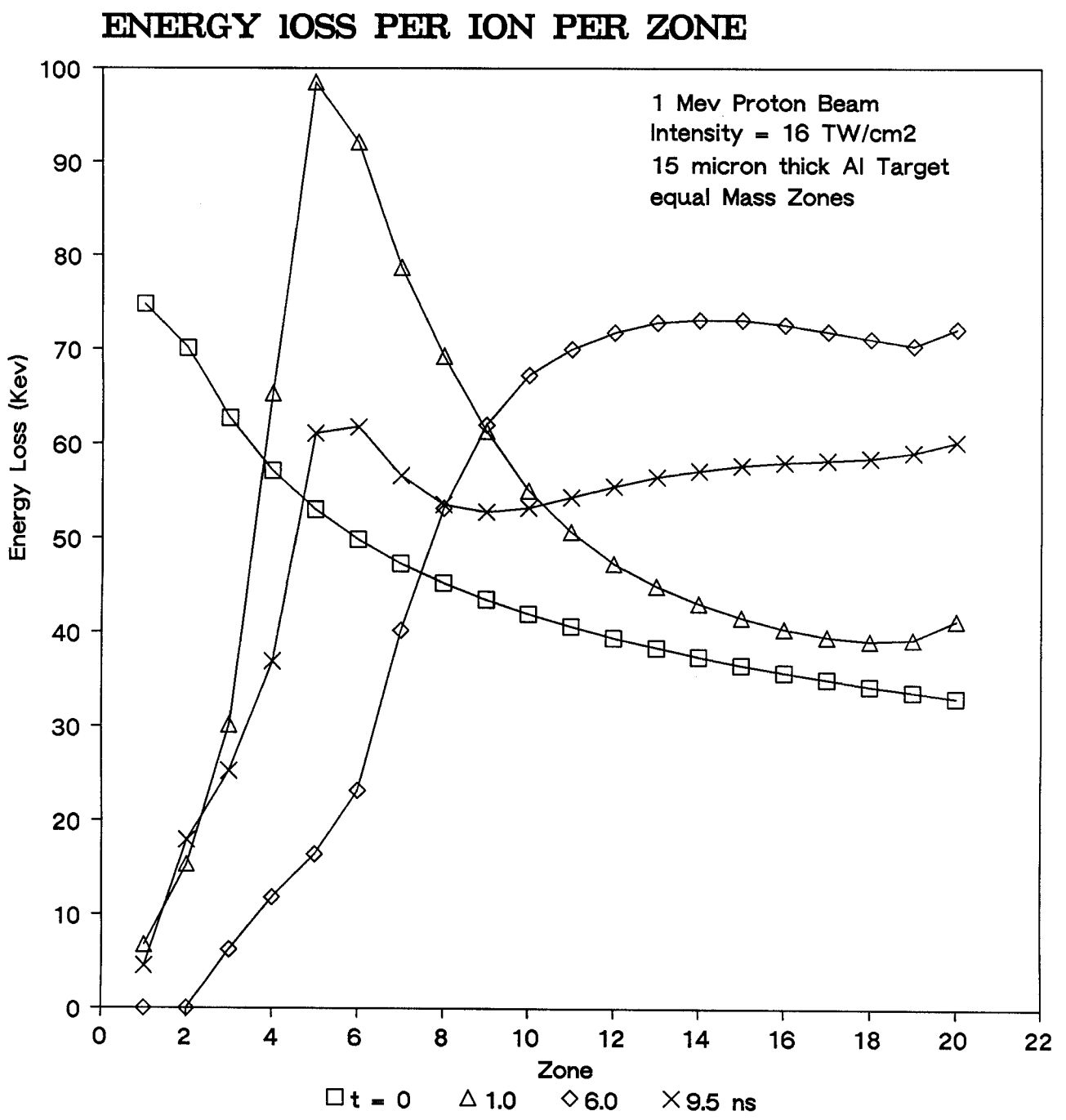

Fig. 4. Energy Lost by Each Ion in Each of the 20 Equal Mass Lagrangian Zones at Various Times for the Conditions Described in Fig. 3. The calculation was done with the MEDUSA-KA code.

zones of 15 μm Al target during the course of simulation without including radiation transport. An understanding of this figure is aided by Figs. 5 and 6 showing the temperature and density profile at different time steps and by Fig. 7 depicting the range shortening and enhancement phenomena as target temperature rises. At the start of the pulse the range of the 1 MeV protons is about the thickness of the target. As the temperature rises, the range shortens to its maximum extent at about 6 ns and starts lengthening again (see also Fig. 7). At the start, due to the Bragg peak, the rear part of the target is heated more strongly than the front surface. After about 1 ns of heating with the 16 TW beam, the temperature rises to about 30 eV and range shortening takes place. It continues up to 6 ns. At this time the temperature of the target rises up to 200 eV and the Bragg peak has almost disappeared. At 9.5 ns, towards the end of the pulse, the range increases again to about its original value but due to the higher temperature the Bragg peak is not as pronounced as at the start. This behavior can also be seen in Fig. 7. Figure 8 shows the front and rear surface temperatures of the target as calculated with MEDUSA-KA without radiation transport. (Results of PHD-IV without using the radiation transport option are essentially the same.) The temperatures reported by NRL are up to 50% higher than those observed in our calculations. This may be attributed to, as is shown in Fig. 9, their use of a simple equation of state and different energy deposition profiles. Rogerson et al. also predicts a slower cooling after the pulse has been shut down. The rise in rear surface temperature (for the no radiation transport case) cannot be seen in our calculation.

In Fig. 10 the temperature of the front surface is compared with those of the NRL publication with and without inclusion of radiation transport. In

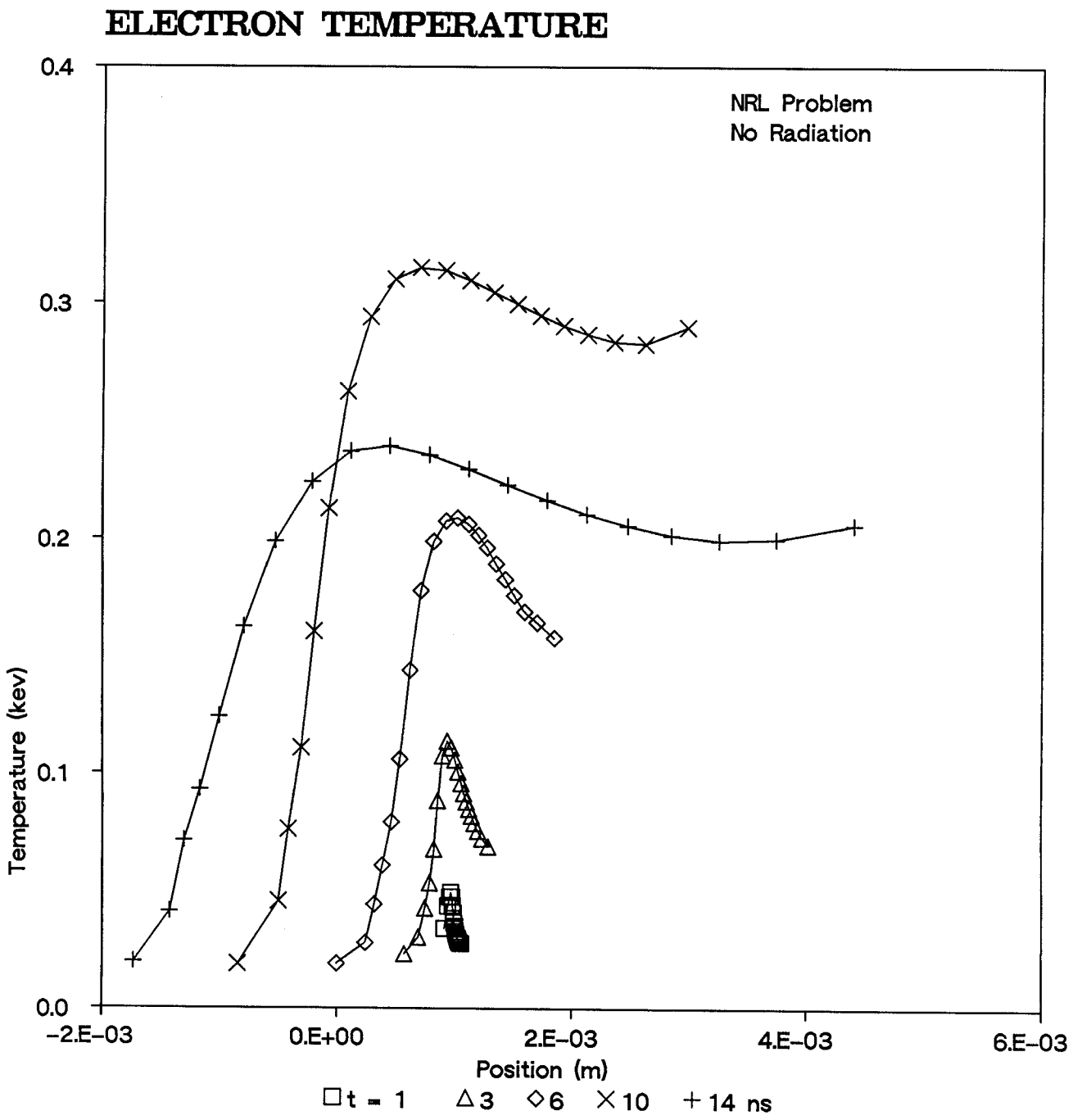

Fig. 5. Electron Temperature Profiles as Calculated by MEDUSA-KA in a 15 μm Thick Solid Aluminum Slab Target at Various Times. The ion beam conditions are the same as described in Fig. 3.

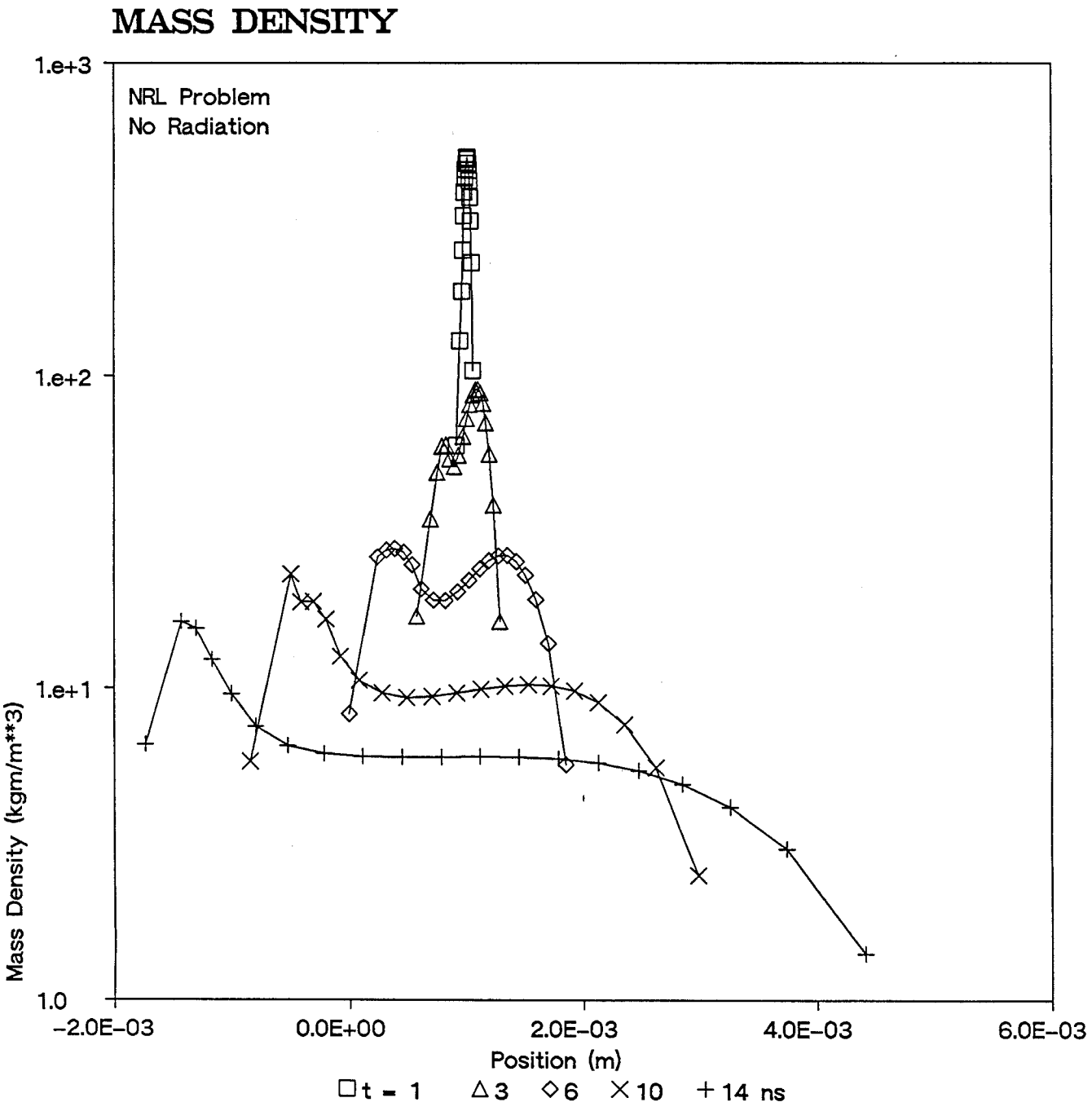

Fig. 6. Mass Density Profiles as Calculated by MEDUSA-KA in a 15 μm Thick Solid Aluminum Slab Target at Various Times. The ion beam conditions are the same as described in Fig. 3.

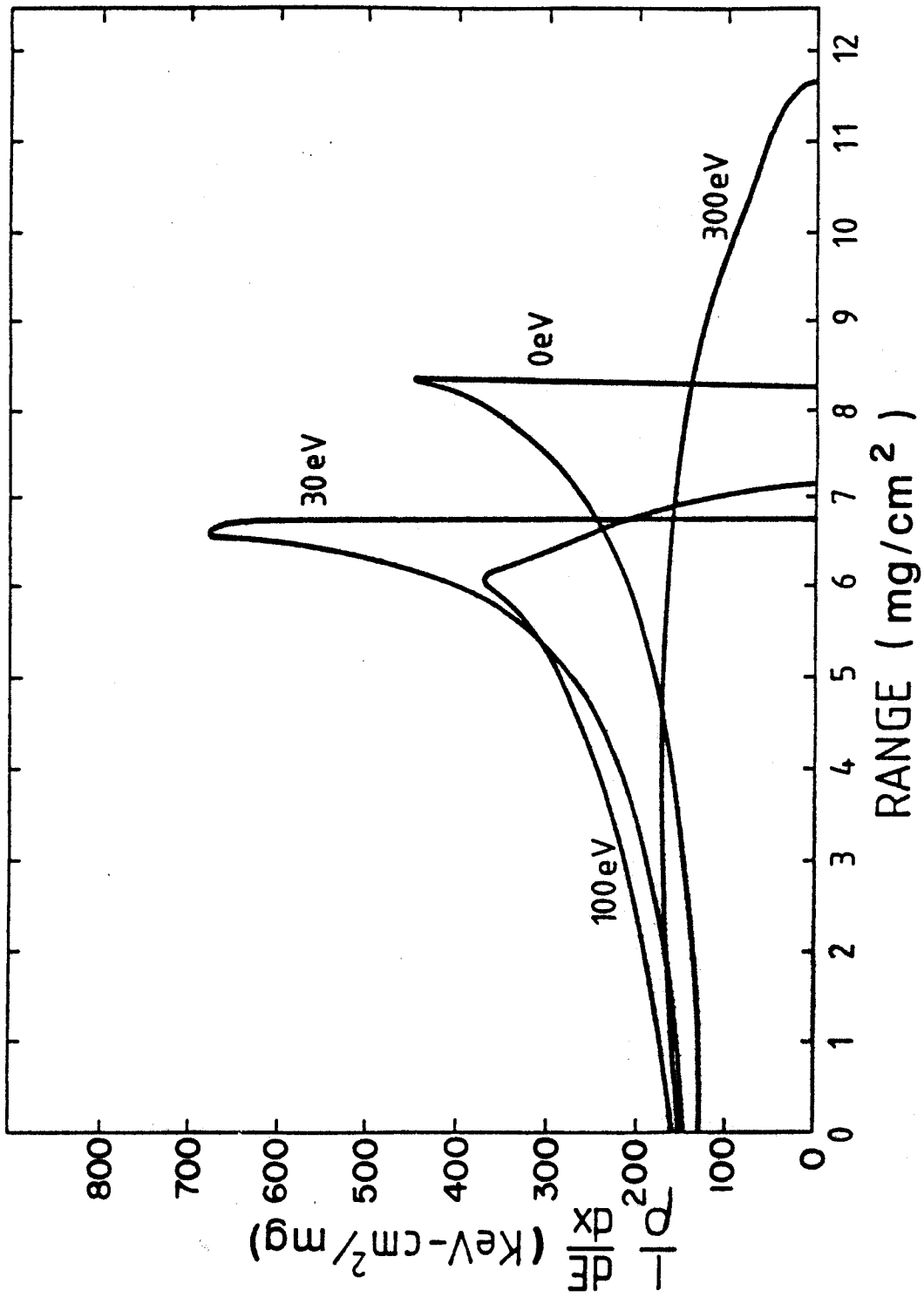

Fig. 7. Proton Stopping Power Profiles as Calculated by MEDUSA-KA in a 15 μm Thick Solid Aluminum Slab Target at Various Temperatures. The ion beam conditions are the same as described in Fig. 3.

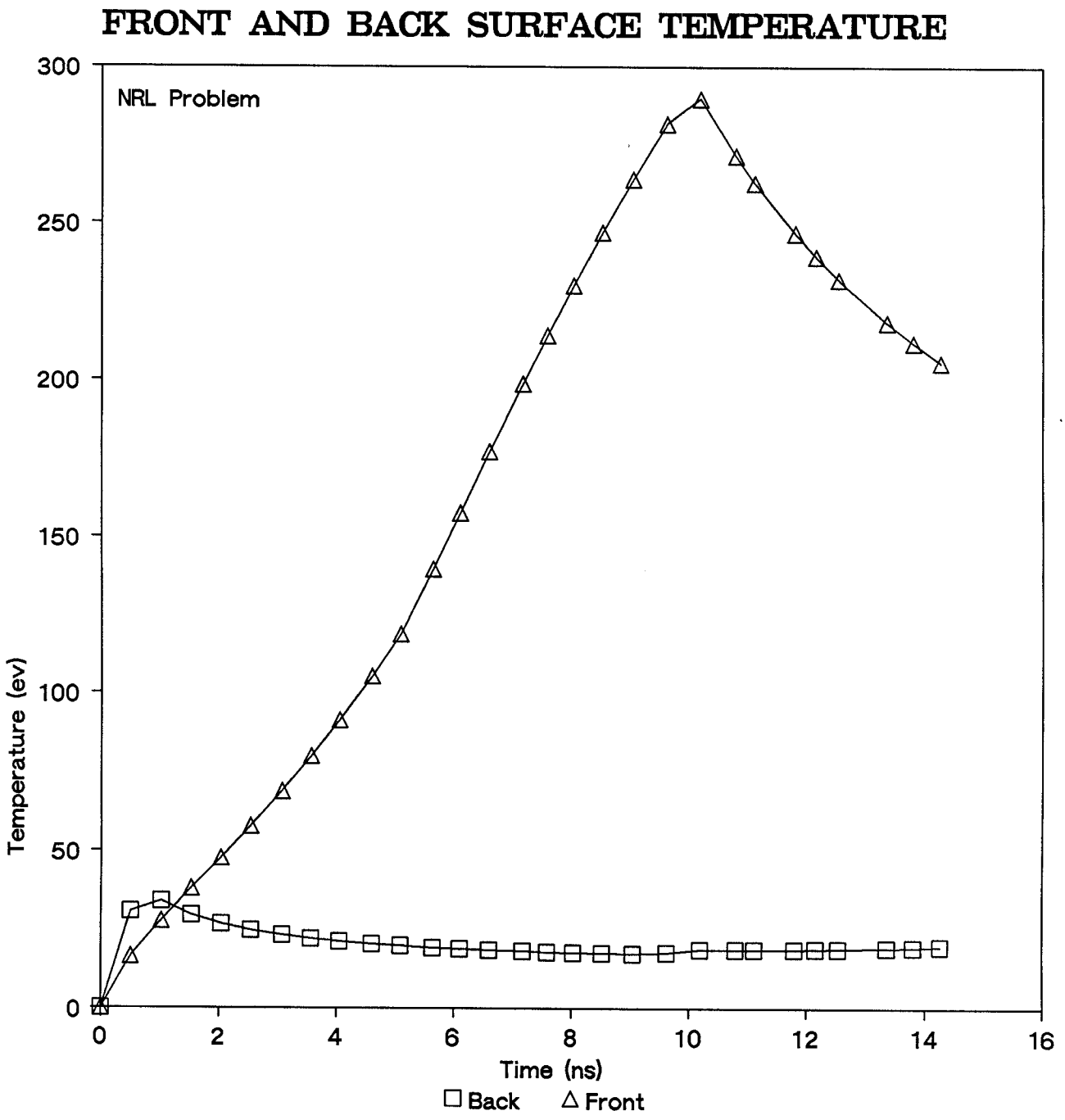

Fig. 8. Temperatures on the Front and Back Surfaces of a 15 μm Thick Solid Aluminum Slab Target as Calculated by MEDUSA-KA versus Time. The ion beam conditions are the same as described in Fig. 3.

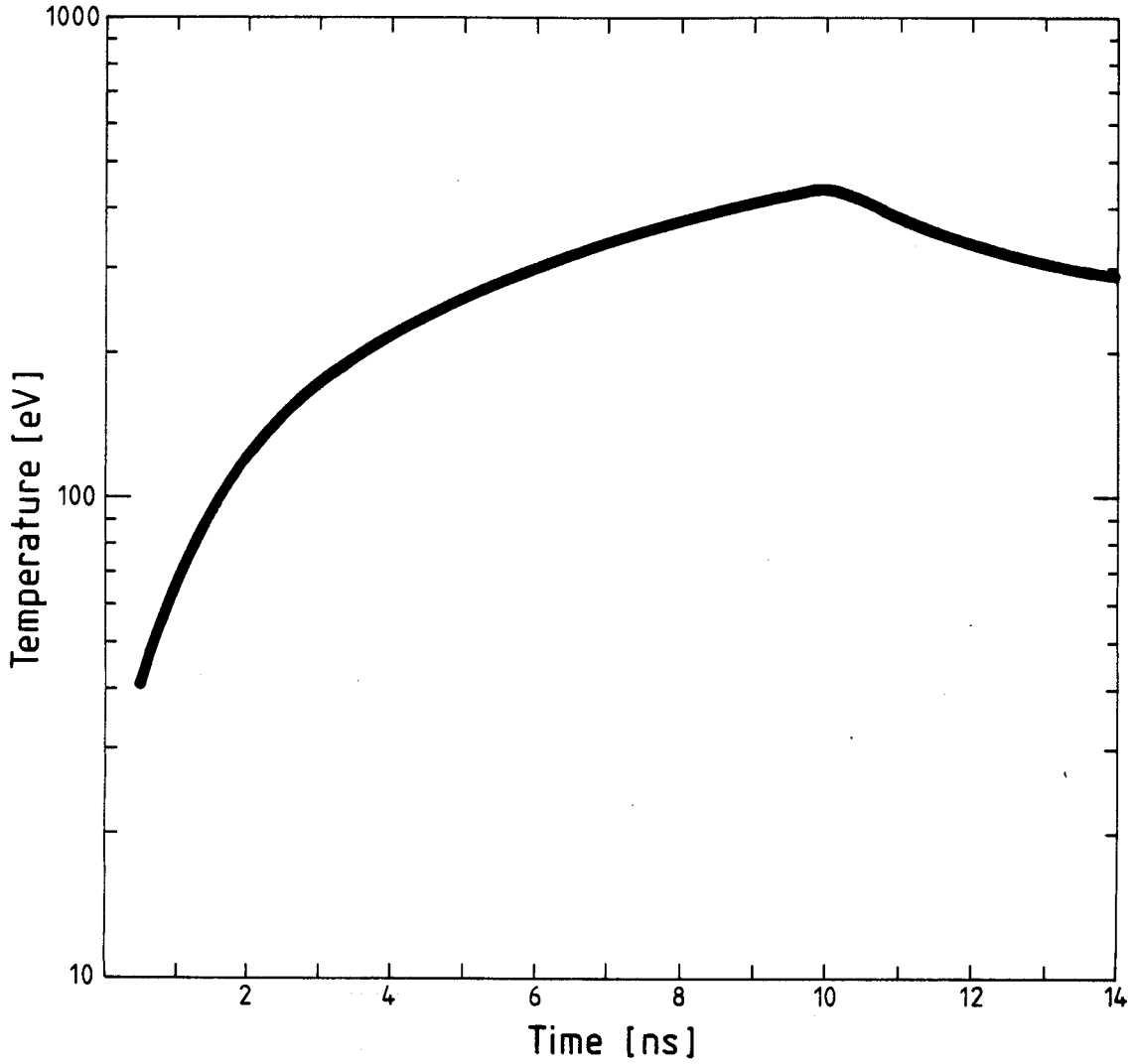

Fig. 9. Front Surface Temperature for Ideal Gas Law Equation-of-State versus Time as Calculated by MEDUSA-KA in a 15 μm Thick Solid Aluminum Slab Target. The ion beam conditions are the same as described in Fig. 3.

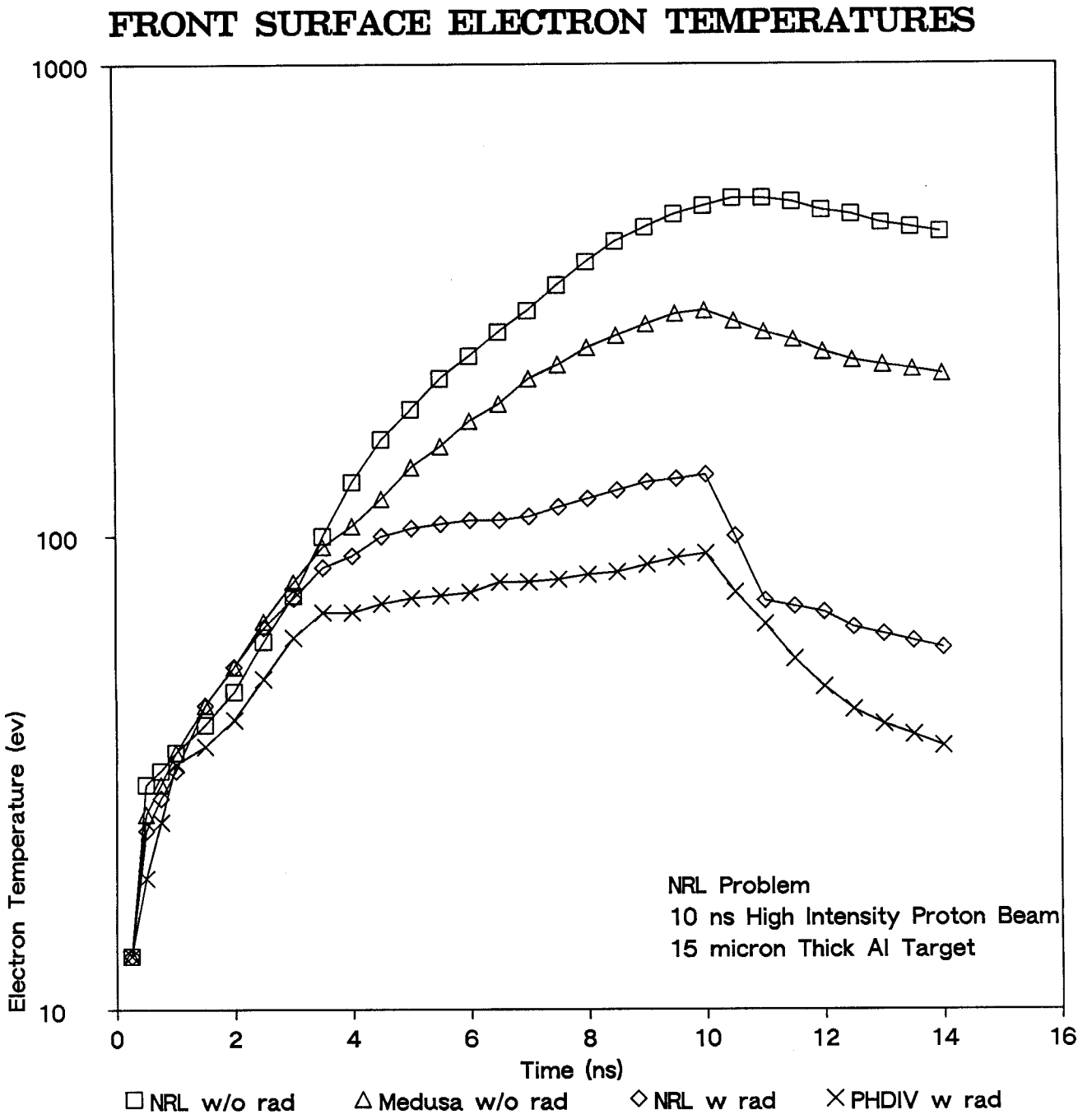

Fig. 10. Front Surface Electron Temperature versus Time in a 15 μm Thick Solid Aluminum Slab Target. Calculations have been done with MEDUSA-KA and PHD-IV, without and with radiation transport respectively, and are compared with published results from NRL. The ion beam conditions are the same as described in Fig. 3.

both cases, the temperatures in our calculations are lower than the NRL calculations. However, both calculations show similar behavior of the temperature. Considering the difference in calculational methods the agreement is considered reasonably good.

Finally, in Fig. 11 spectra of radiation emitted from the front surface of the aluminum target at different times are given. The multigroup radiation transport cannot give details of line radiation but the overall shape of emitted spectra compares well with those of Rogerson et al.

An important difference in the NRL and our calculations is the equation of state and ionization state of the target. Figure 9 shows the result of a MEDUSA-KA calculation for the front surface temperature with the same parameter as in Figs. 8 and 10 except that now an ideal gas equation of state is used. In agreement with the NRL results, temperatures as high as 400 eV are observed. The rapid rise in temperature at earlier times is due to the neglect of ionization energy with the ideal gas equation of state. This was included in the NRL calculation. The effect of ionization energy is stronger at lower temperatures when the degree of ionization changes rapidly.

The NRL calculations have used an average degree of ionization throughout the course of beam irradiation. This may not be a valid approximation, since, as shown in Fig. 12 (borrowed from Ref. 25) the range of 1.6 MeV protons changes strongly with degree of ionization.

V. PLANNED EXPERIMENT OF KALIF

The 16 TW beam power used in the above benchmark calculations is more than an order of magnitude higher than the light ion beam power that can be reached with the present KALIF machine. The idealized square pulse is also of an academic interest. The shape of the ion beam pulse would look somewhat

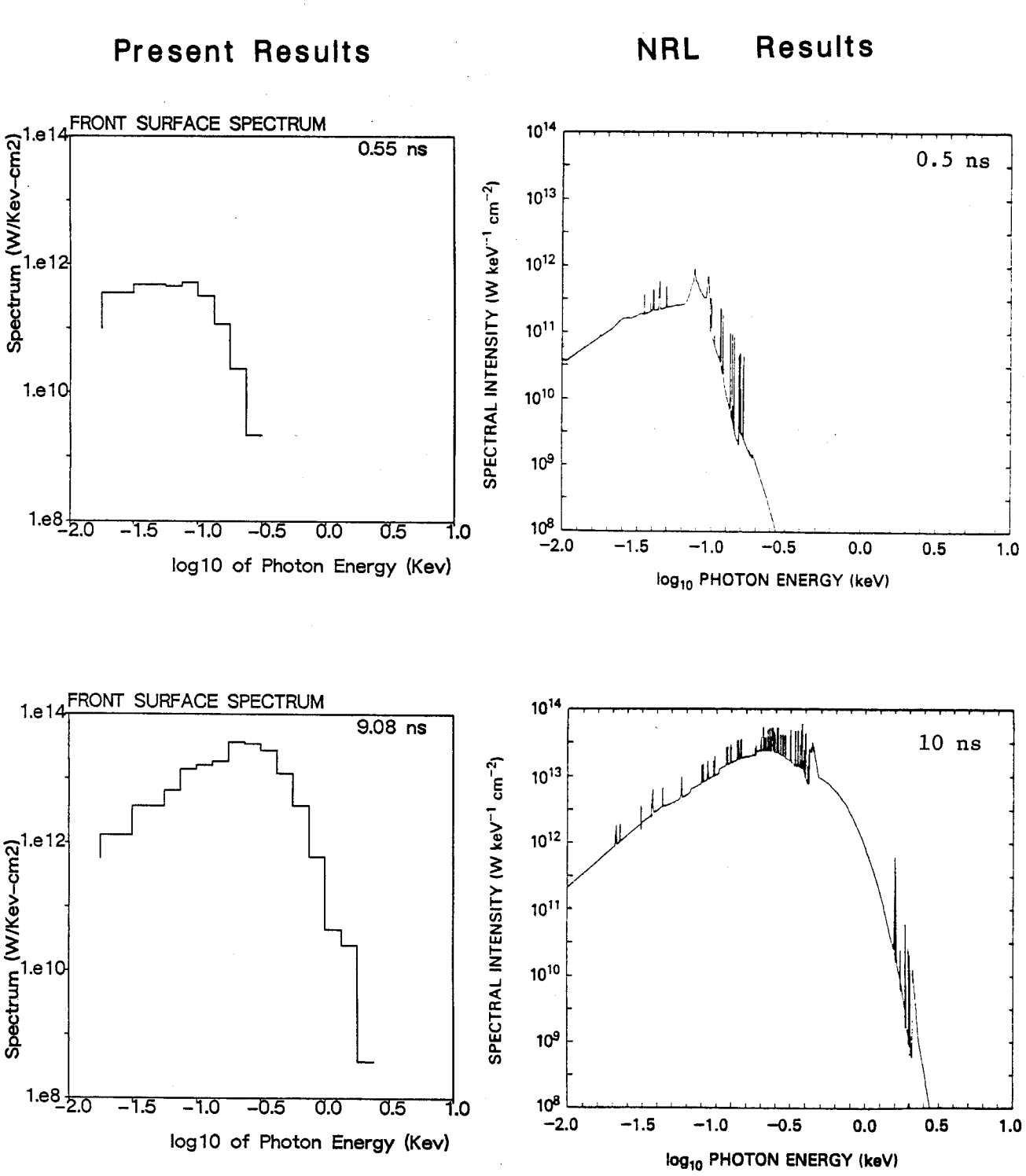

Fig. 11. Spectra of Radiation Emitted from the Front Surface of a 15 μm Thick Solid Aluminum Slab Target at Various Times. Results of calculations done with PHD-IV, which uses multigroup radiation diffusion, are compared with results from NRL. The ion beam conditions are the same as described in Fig. 3.

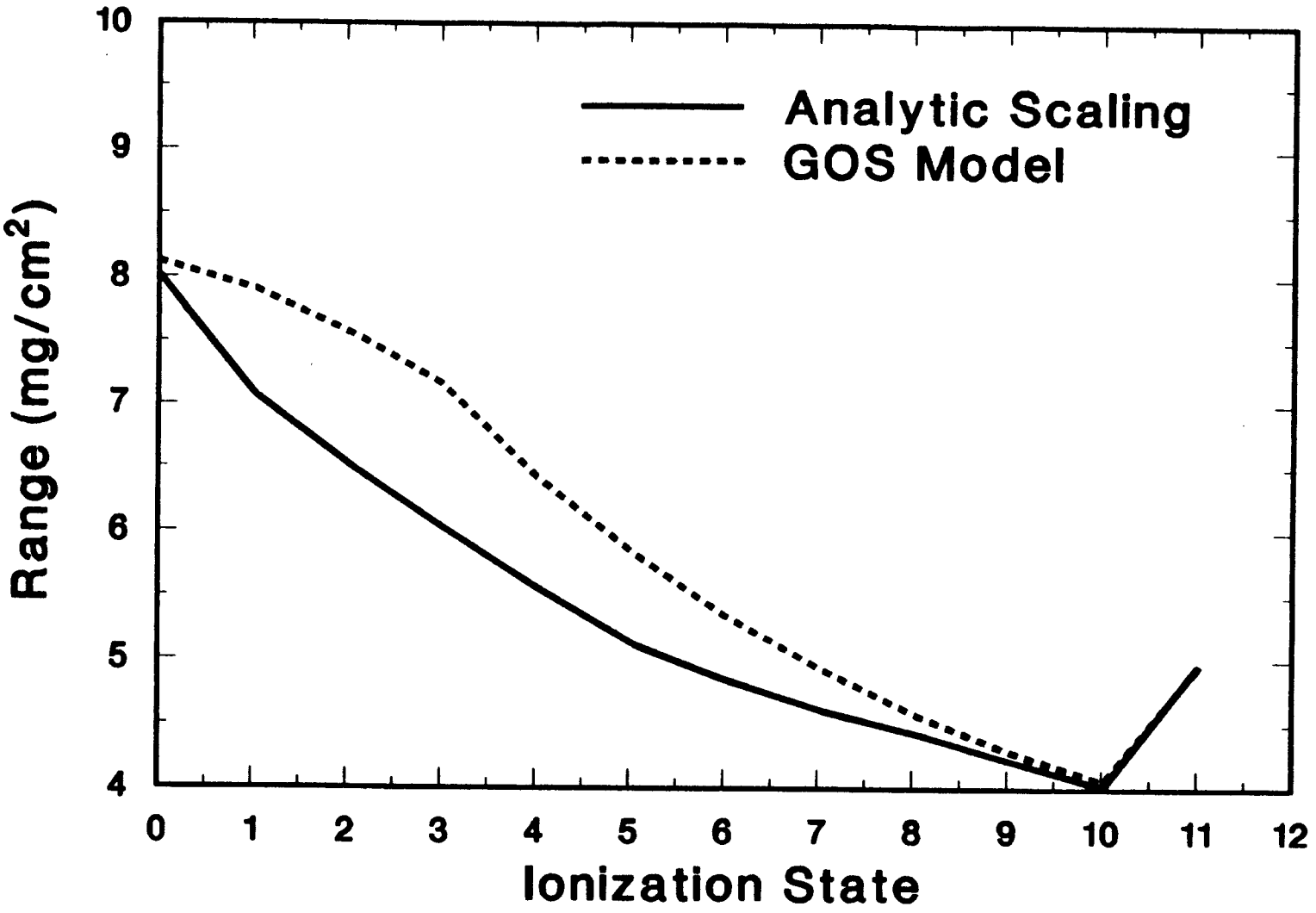

Fig. 12. Range of a 1.6 MeV Proton in Aluminum versus Ionization State (from Ref. 25).

like Fig. 13. Both voltage and current change with time. The ion beam also does not always hit the target normally as assumed in the previous section. Experiments are therefore planned at KfK to measure dE/dx in hot plasmas. But due to the geometry of the anode and ballistical focusing, the angle of incidence varies according to the diode characteristics. The codes MEDUSA-KA and PHD-IV were modified to accommodate these effects.

A possible experimental setup to measure proton stopping power at KALIF is shown in Fig. 14. In the diode, ions are emitted from the anode, accelerated in the anode-cathode gap, charge neutralized as they pass through a thin plastic foil bounding the drift tube, and are ballistically focused. The ion beam is scattered before and after passing through the target, which is chosen for the following analysis to be 7.5 μm thick aluminum foil. Both the beams pass through the magnetic field analyzer and a streak camera permits a simultaneous measurement of beam energy as it enters and leaves the target.

VI. PRE-EXPERIMENTAL CALCULATIONS

Figure 13 shows the characteristics of a pinch reflex diode presently used at KALIF.[8] For the following calculations it is assumed that these profiles are transferred to the ion beam without appreciable distortion and the angle of incidence on the target is 14°. It is recognized that the ion current will be much less than the total diode current. The total power assumed on the target is 0.4 TW/cm^2. For the present calculation a 7.5 μm (2 mg/cm^2) thick aluminum slab target is used. The thickness is about a quarter of the range of 1.5 MeV protons in cold material. As will be shown later, this target allows the measurement of proton stopping in aluminum from about 3 eV to 25 eV.

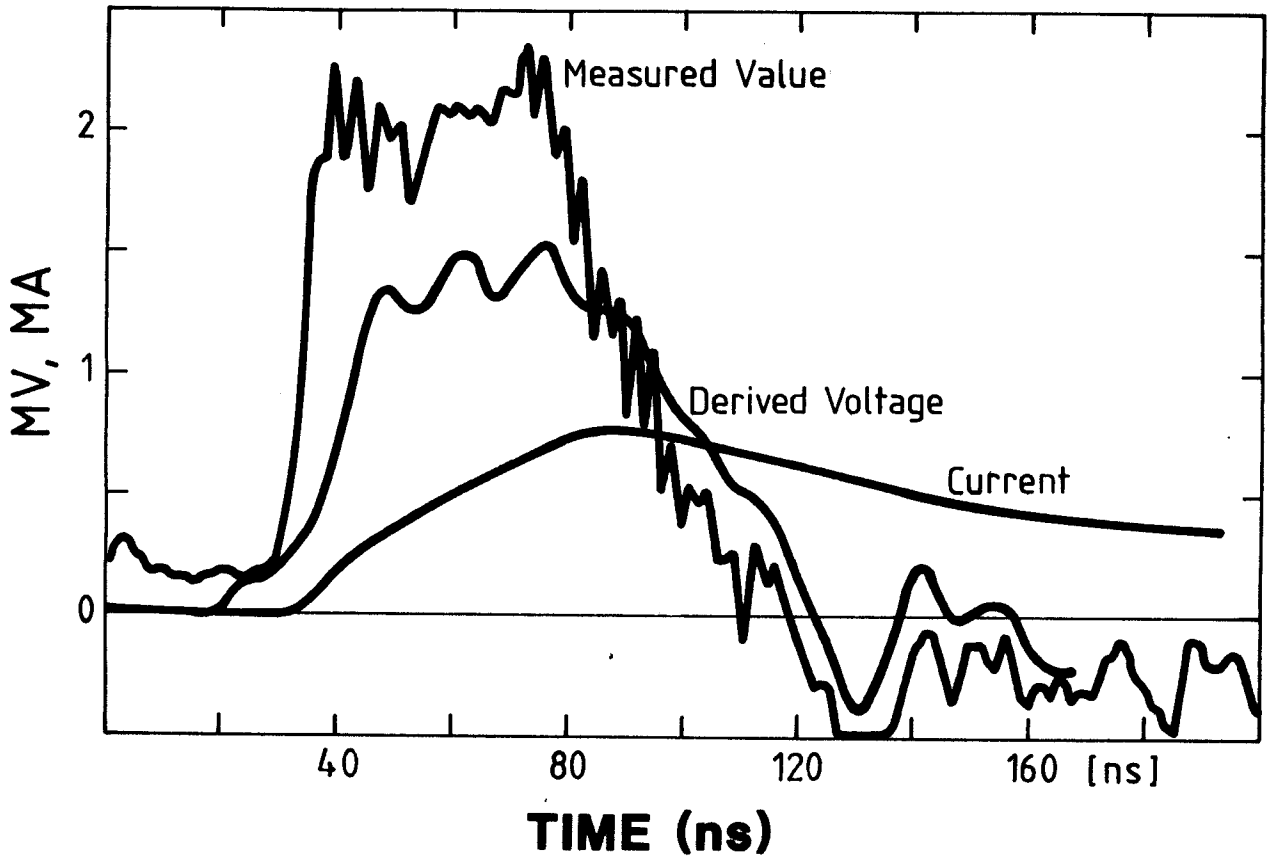

Fig. 13. Measured and Derived Voltage and Current in an Ion Diode on KALIF.

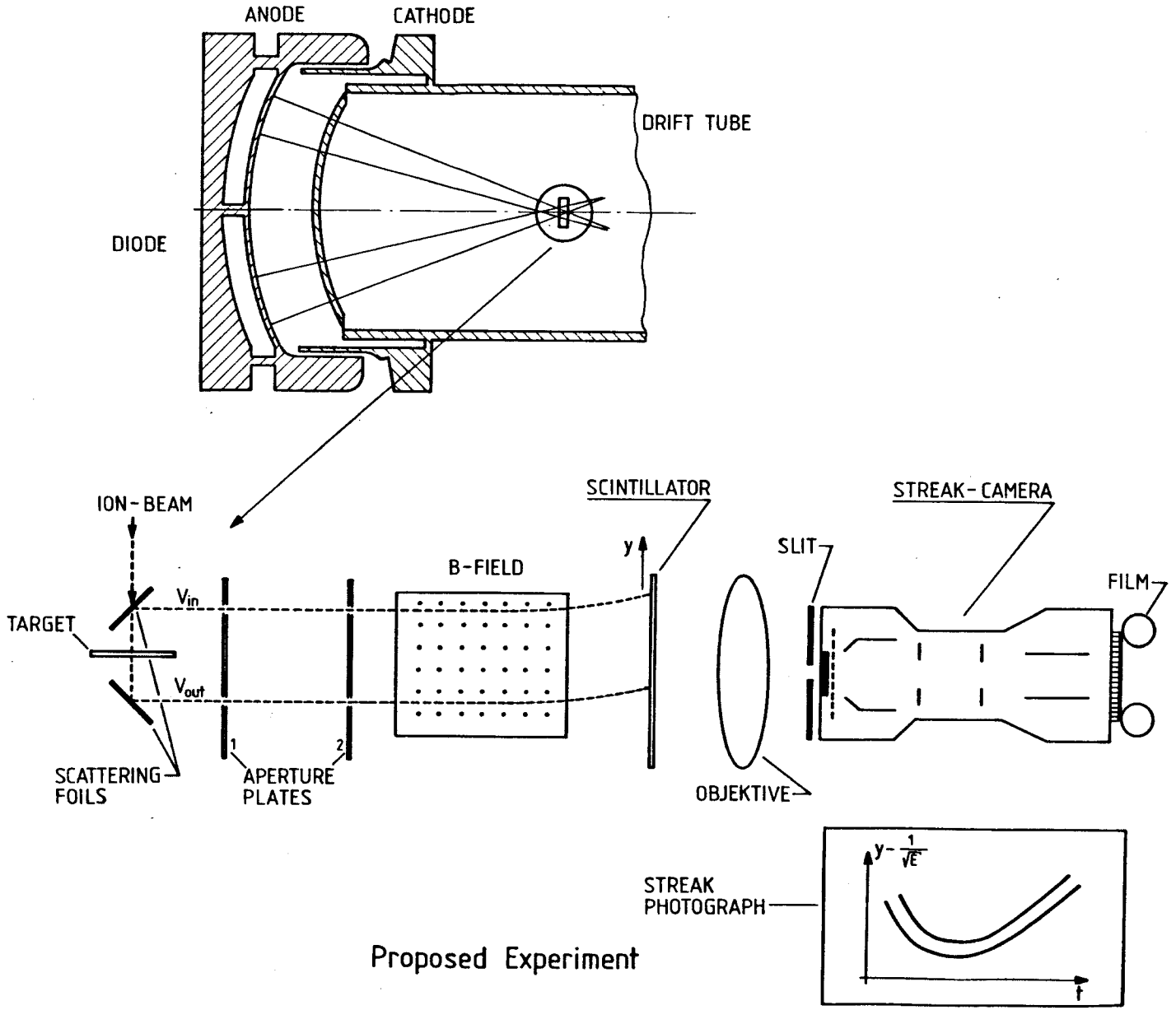

Fig. 14. Schematic of Proposed Experimental Setup to Measure on KALIF.

Figure 15 shows the evolution of temperature and density of the target midplane with time. Also shown is the incident beam power. (Please note that the time scale in the hydro calculation is different than in Fig. 9. Hydro calculations start at the point when power coming out of diode is different from zero.) The basis of this figure is a MEDUSA-KA calculation without radiation transfer. At these temperatures this omission makes little difference except at the end of the pulse, at times where the ion stopping measurement is not possible anyway. If the ion beam would start at 1.5 MeV instantaneously the target would be heated uniformly and the dE/dx measurement could start right from the beginning. However, at the initial stages, the beam voltage, and thus the ion energy, are so low that the Bragg peak in the ion stopping heats the target nonuniformly. At about 10 ns the target temperature profile becomes fairly uniform and as seen in Fig. 16 remains so throughout the course of the experiment. The density profile, shown in Fig. 17, is parabolic because outer zones expand more quickly than the center of the target. This confirms results of the analytical calculations of Ref. 5. However, in Ref. 5 even for the idealized conditions, square pulse, constant energy deposition, a nonuniform temperature profile is predicted. Figure 14 of Ref. 5 is drawn at a time of 1.3 ns. This time is far shorter than the time a sound wave would travel across the target, therefore a stable condition is not yet reached. At 10.2 ns (Fig. 15 of Ref. 5), however, the temperature profile is almost flat. The small drop in temperature on the boundary may be caused by the special radiation loss assumption used in that reference. Figure 18 shows the incoming beam energy and the energy with which particles leave the rear surface of the target. Also shown are the results of calculations with the GORGON code for three different time steps, using the average temperature and

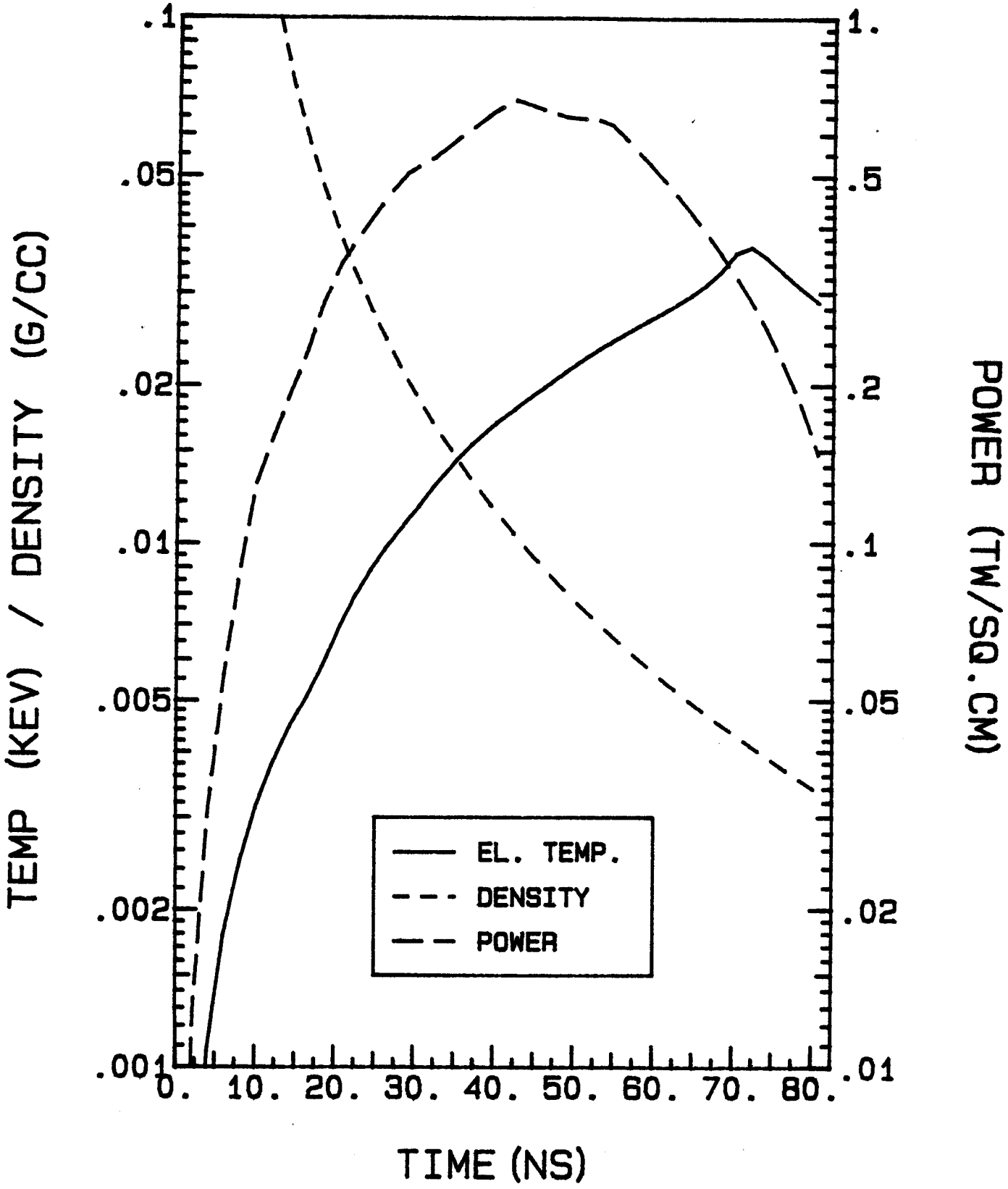

Fig. 15. Midplane Density and Electron Temperature and Incident Ion Beam Power Density in KALIF Experiment. The incident beam consists of protons with a maximum energy of 1.5 MeV and the target is a 7.5 μm thick aluminum foil.

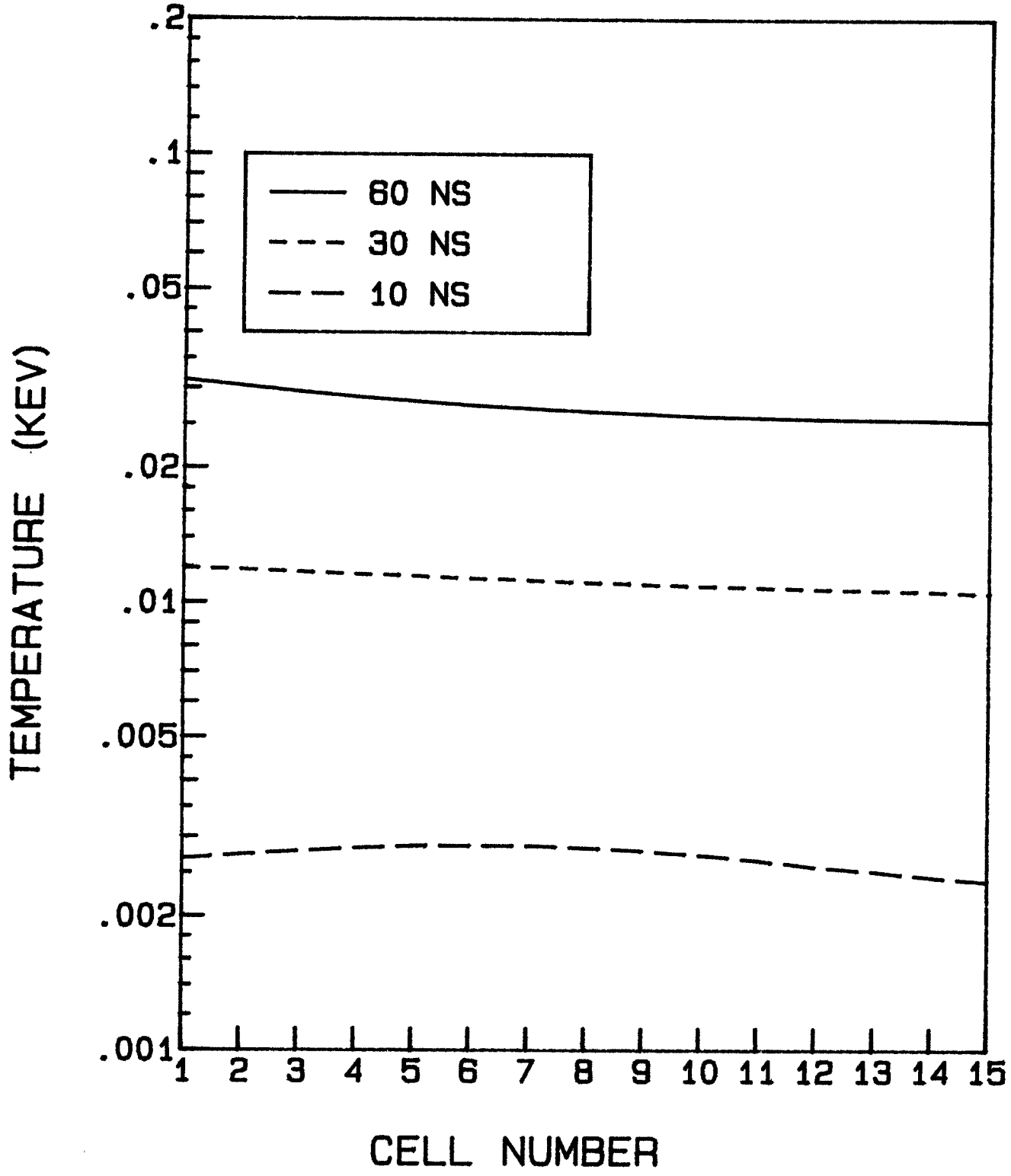

Fig. 16. Electron Temperature Profiles in 7.5 μm Thick Aluminum Target at Various Times. The ion beam is the same as in Fig. 15.

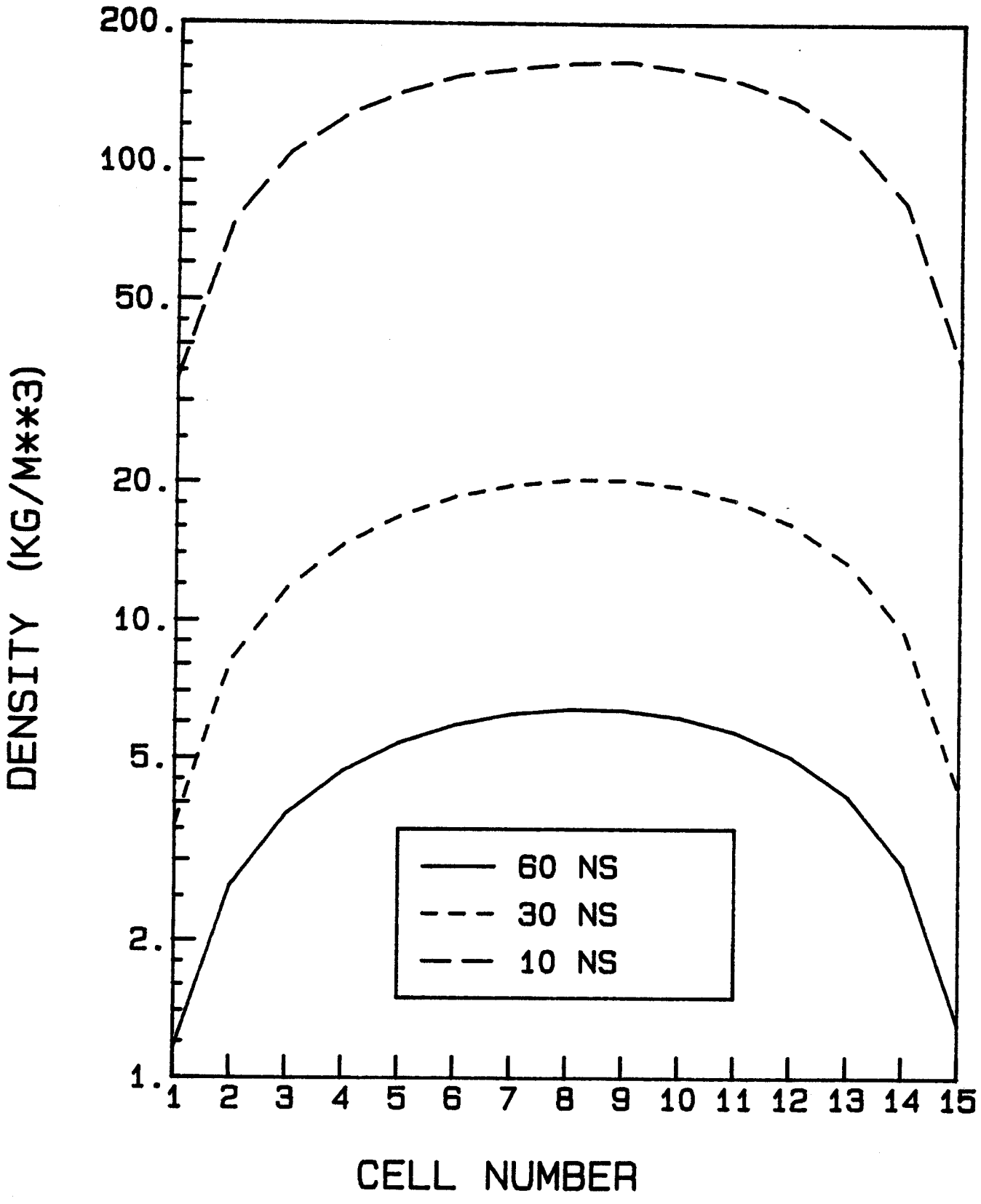

Fig. 17. Mass Density Profiles in 7.5 μm Thick Aluminum Target at Various Times. The ion beam is the same as in Fig. 15.

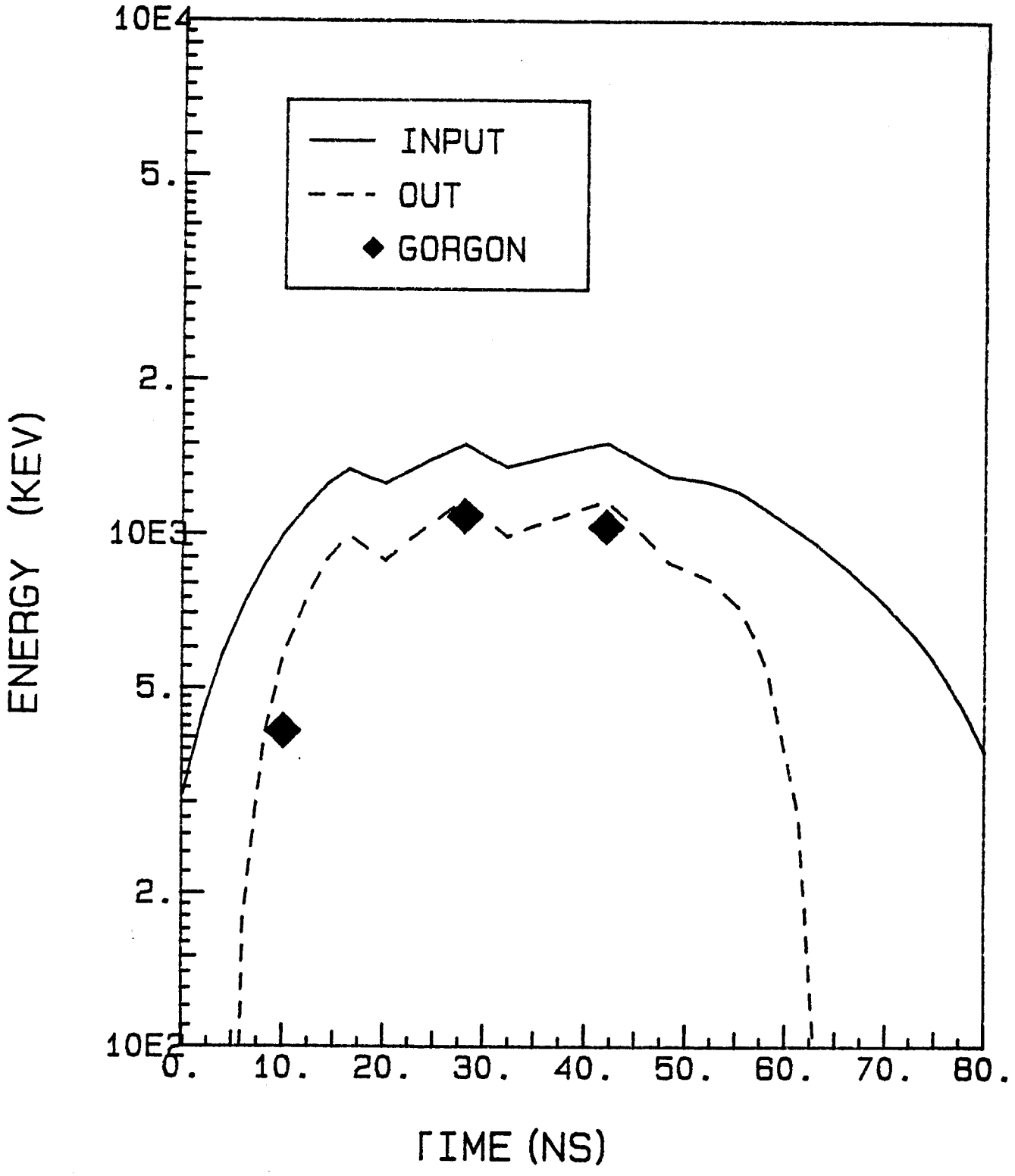

Fig. 18. Energies of Ions Entering and Leaving a 7.5 μm Thick Aluminum Target at Various Times. Also shown are the energies of ions leaving the target at three times as predicted by the GORGON code. The ion beam is the same as in Fig. 15.

density. It is seen that the agreement with the basic GORGON code and a more simple method incorporated in the hydro code is very good.

Because of the low energy the beam does not penetrate out of the target for the first 5 ns. In fact a meaningful measurement may not be possible prior to 10 ns. At this time the temperature of the target has reached 3 eV and the input beam energy is 1 MeV. The measurement can be continued until about 55 ns at a time when the temperature of the target is 28 eV. Radiation losses are not important at these temperatures. Figure 19 also demonstrates the enhancement of stopping power due to temperature and density changes. For example at 10 ns, out of 1 MeV input energy, only 420 keV is deposited in the target ($T = 3$ eV and $\rho = \rho_s/20$) whereas at 60 ns the input energy is again 1 MeV. The energy lost in the target is 730 keV, almost double the previous value. At this time the temperature is $\approx$ 30 eV and $\rho = \rho_s/500$. In a one-dimensional slab target the ρR value of the target remains constant as the target expands. Thus in this experiment stopping enhancement should be clearly observed.

The results presented so far assumed that the particle beam is purely protons, but in fact the beam is always contaminated with other particles. At KALIF, the beam was observed to contain only 87% protons, with the remainder being carbon; namely 3% C^{+}, 8% C^{+2} and 2% C^{+3}. Since dE/dx is proportional to Z^2 the range of carbon ions is much shorter than protons. They are stopped in the first 1/3 of the target, thereby raising the temperature of the front surface dramatically; this is clearly shown in Fig. 20. In the calculation without radiation transport temperatures higher than 100 eV are predicted. At these temperatures, ignoring the radiation is not a good approximation. Calculations were repeated with radiation transport included using the PHD-IV

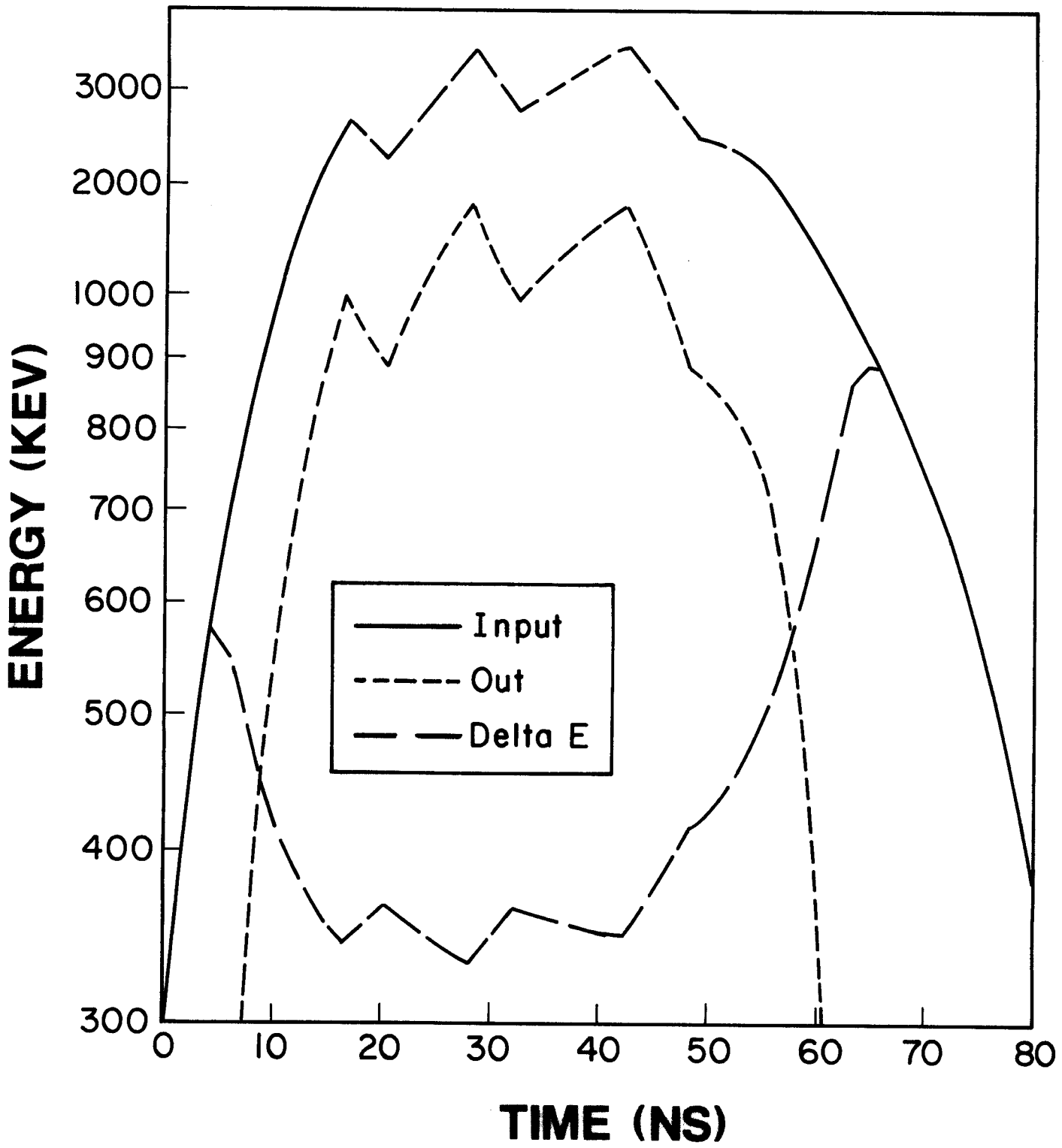

Fig. 19. Energies of Ions Entering, Leaving and the Energy Lost by Ions while Traversing a 7.5 μm Thick Aluminum Target at Various Times. The ion beam is the same as in Fig. 15.

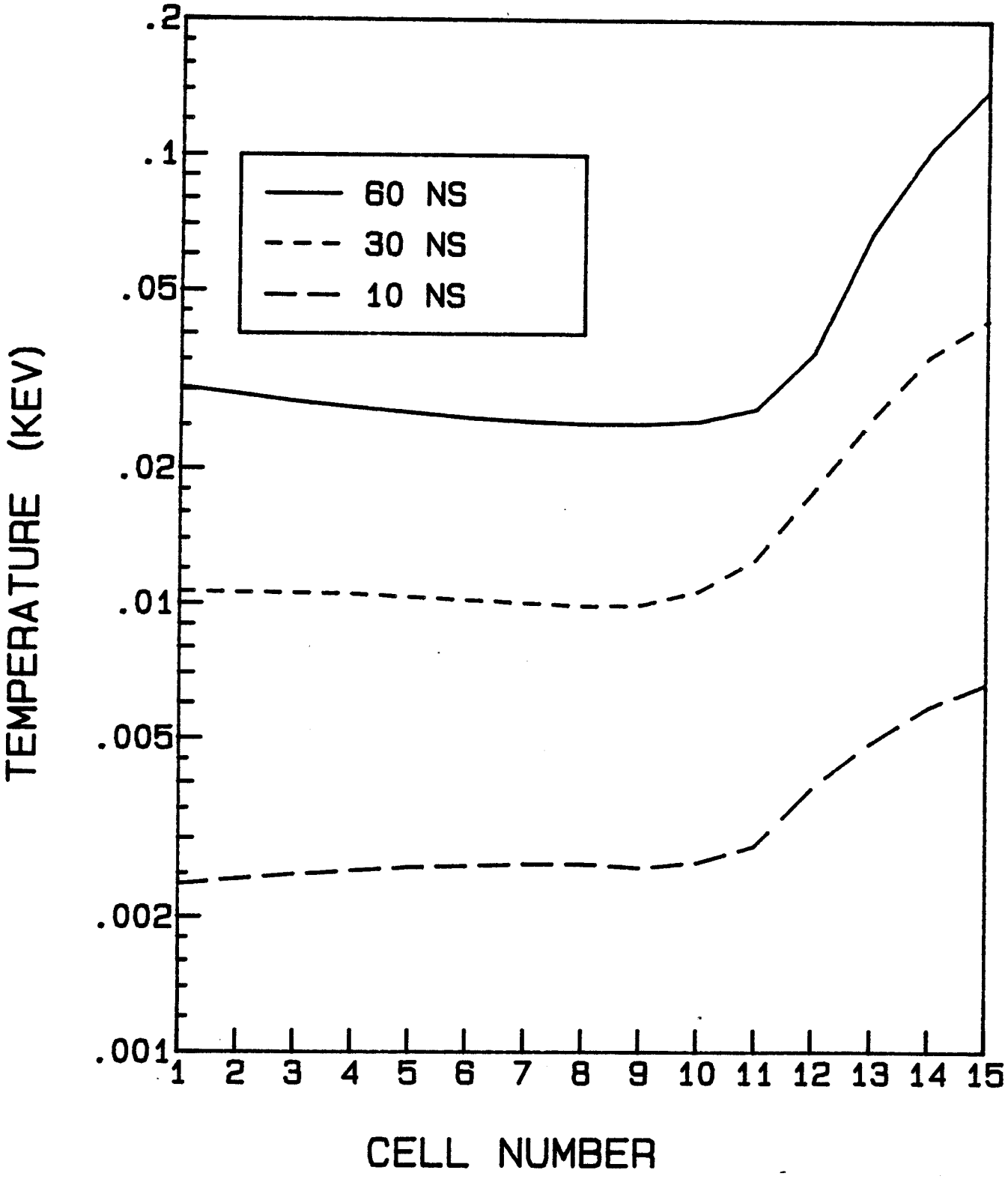

Fig. 20. Temperature Profiles in a 7.5 μm Thick Aluminum Target at Various Times. The beam power and diode voltages are the same as in Figs. 15 through 19, but it is 87% protons, 3% C^{+}, 8% C^{+2}, and 2% C^{+3}. Radiation transport is not considered.

code, which are shown in Fig. 21. The extremely high temperatures at 33 and 60 ns, for example, have been lowered due to radiation cooling. At 60 ns the temperature profile is almost as flat as in the case of a proton beam only. However at earlier times the flatness of the temperature profile has been destroyed due to the carbon contamination of the beam. There is not enough energy in the radiation field to smoothen the temperature profile. This is evident from Fig. 22 which shows the energy partitioning in the target.

VII. DISCUSSION OF RESULTS

Results presented in Section IV show a reasonable agreement between our code predictions and those of Rogerson et al. At the beam power level of 16 TW both phenomena of range shortening and range lengthening can be observed. At this power level, radiation transport is very important. Our multigroup treatment of radiation transport compares with their continuum spectrum. However, we cannot obtain any detailed information about the line radiation. The main difference between our predictions and those of Rogerson et al. is in the electron temperature. We believe that this is due to different equations of state.

At the Karlsruhe Light Ion Facility KALIF, dE/dx measurements can be done as a function of temperature in a temperature range of 3 eV to 25 eV for protons of energies 1 MeV and higher. The densities associated with these measurements are 1/30 to 1/500 of the solid state density. The present beam characteristics of KALIF would allow the dE/dx measurement at uniform target temperatures. However, to achieve this, carbon ions must be removed from the beam. This can be accomplished by putting a thin foil in front of the aluminum target. This foil can also be used as a Rutherford scattering diagnostic to measure the energy of the particle beam entering the target foil. Radi-

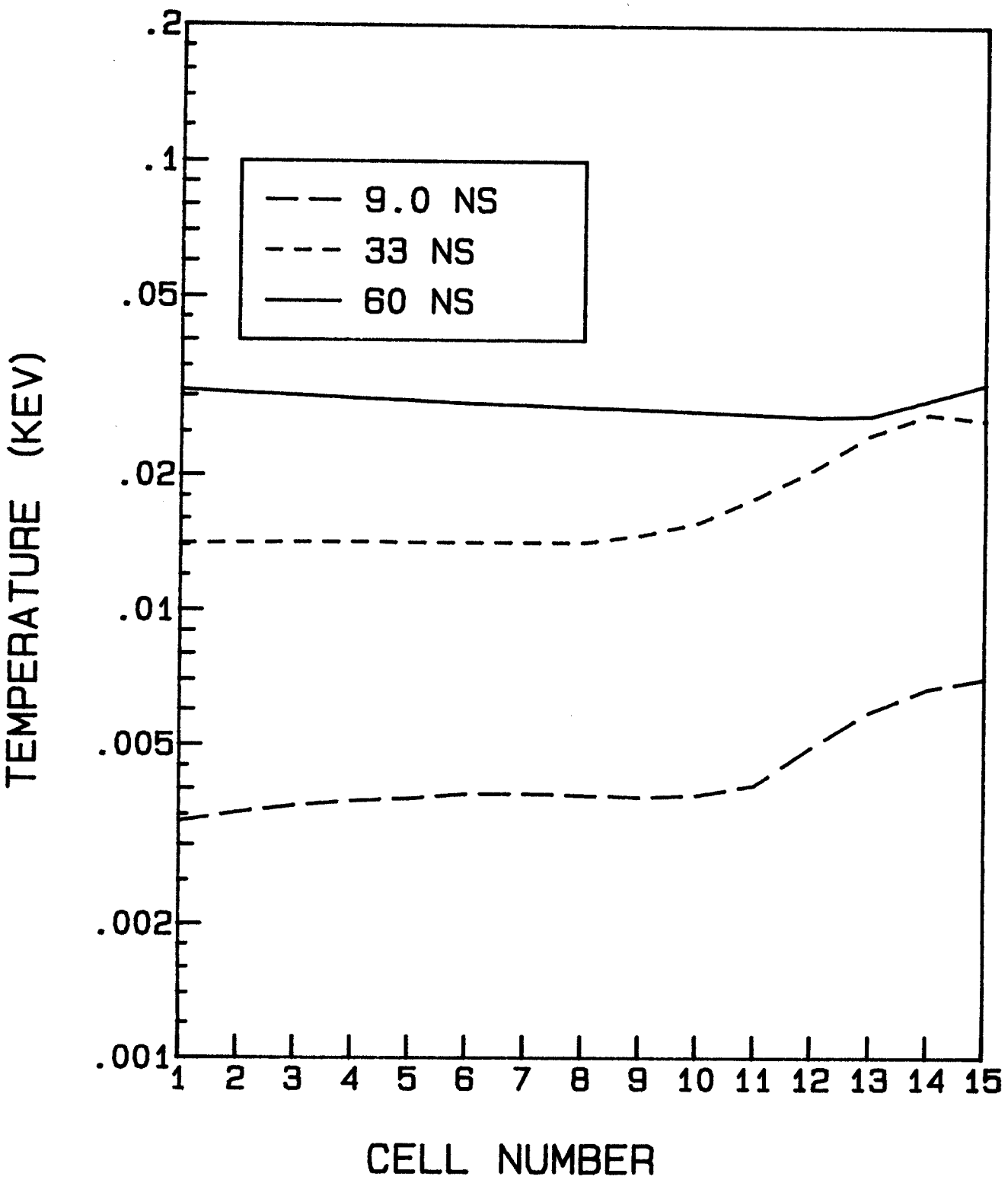

Fig. 21. Temperature Profiles in a 7.5 μm Thick Aluminum Target at Various Times. The beam power and diode voltages are the same as in Figs. 15 through 19, but it is 87% protons, 3% C^{+}, 8% C^{+2}, and 2% C^{+3}. Radiation transport is considered.

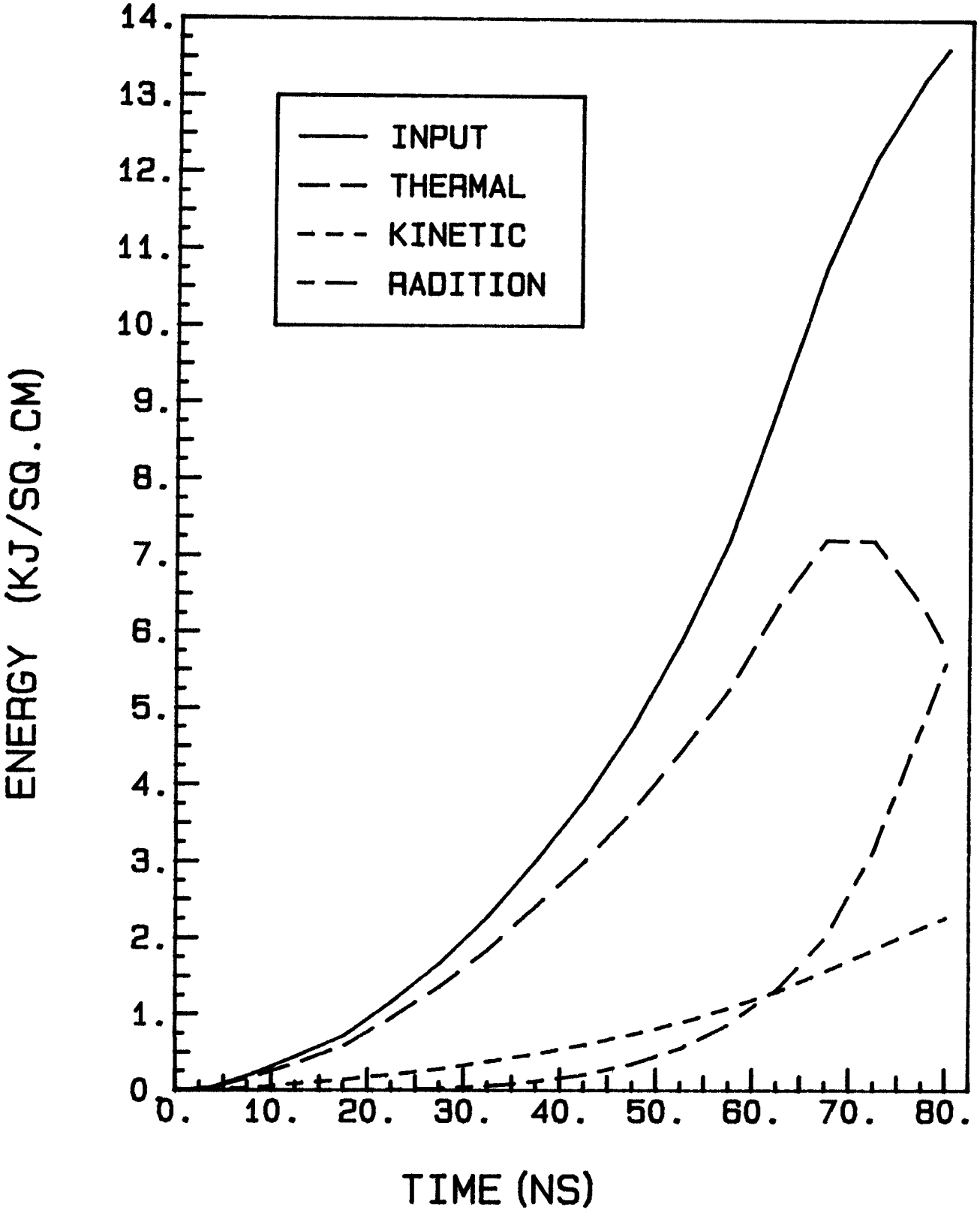

Fig. 22. Energy Partitioning between Thermal, Kinetic, and Radiation and the Total Input Energy in a 7.5 μm Thick Aluminum Target versus Time. The beam power and diode voltages are the same as in Figs. 15 through 19, but it is 87% protons, 3% C^{+}, 8% C^{+2}, and 2% C^{+3}.

ation effects are not important at the present power density of about 1/2 TW/cm^2. The results of the energy stopping formalism included in the hydro codes, MEDUSA-KA and PHD-IV, match very well with the results of GORGON.

Another experiment of this type was performed at the Proto-I accelerator of Sandia National Laboratory and has been published recently.[7] The basic trend of our calculations match well with results published by Olsen et al.[7] However, the temperature and density profiles are not given in Ref. 7. The proton beam at KALIF has a purity of about 90% whereas at Proto-I about 50% of the beam is reported to be nonprotonic.

Figure 14 sketches an experiment being proposed for the dE/dx measurement at KALIF. The ion beam comes from the top. The scattering foil "A" will stop the carbon ions and scatter a part of the beam into the magnetic analyzer. After undergoing interaction in the target, scattering foil "B" scatters the beam again into the analyzing magnets. Apertures 1 and 2 collimate the beam. The scintillation signals are registered in a streak camera. This arrangement would allow the measurement of both incoming and outgoing beam energy.

It is planned to improve the power density at KALIF (a) by improving the pulse compression with the help of plasma erosion switches, and (b) by improving the diode performance. We have repeated the calculations with these changes. A pulse compression is considered, with the associated voltage doubling. Figure 23 shows the energy partitioning. It is seen that in spite of a power increase, only 4 kJ/cm^2 of energy is coupled to the target, instead of 14 kJ/cm^2. This is due to the fact that increased beam voltage lowers the dE/dx value. Accordingly, the temperature range of measurement has been lowered to 0.5 eV to 15 eV. This is shown in Fig. 24, where the midplane density and temperatures are plotted against time. A calculation was also

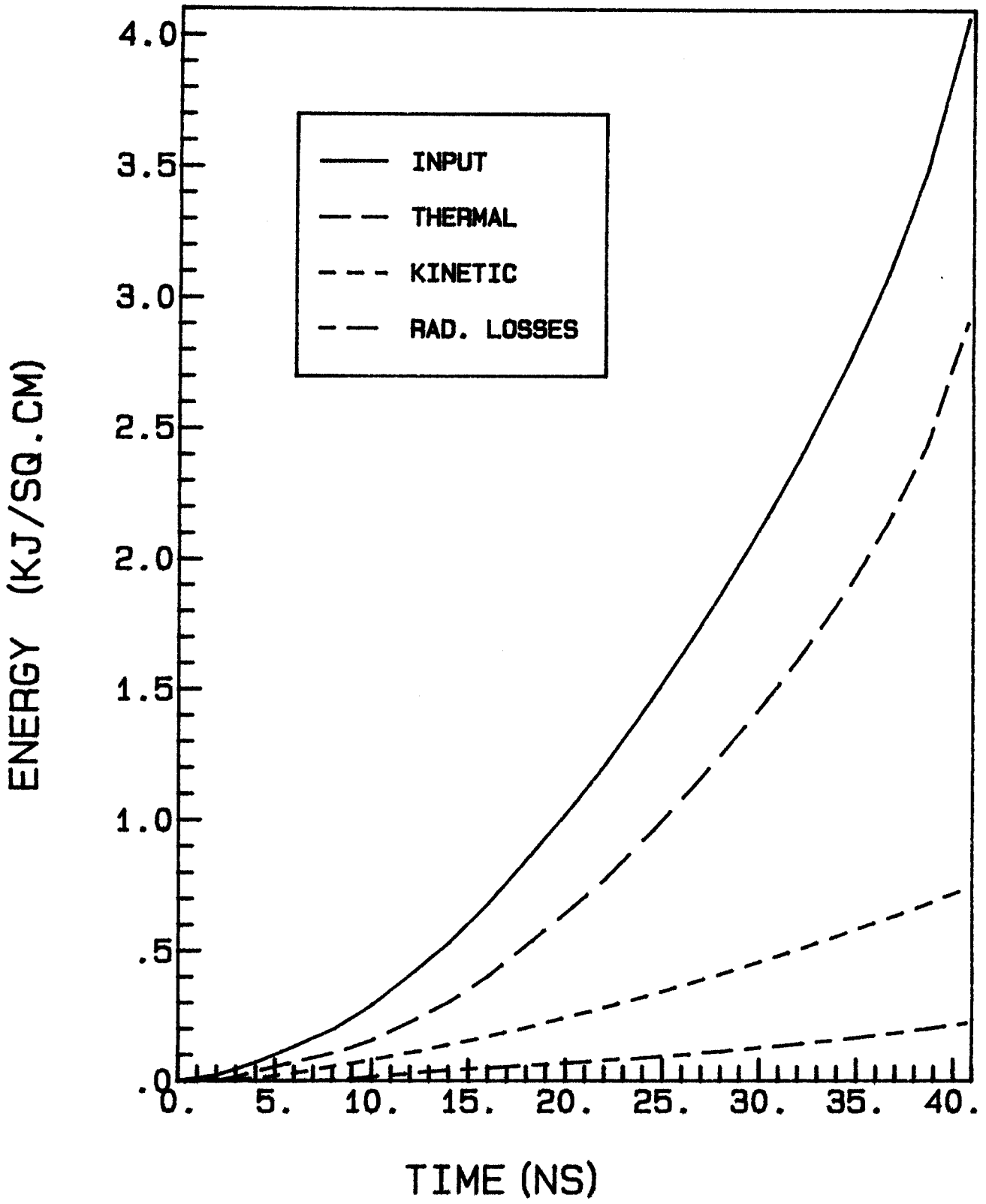

Fig. 23. Energy Partitioning between Thermal, Kinetic, and Radiation and the Total Input Energy in a 7.5 μm Thick Aluminum Target versus Time. The species are the same as in Fig. 22, but the pulse has been compressed and the diode voltage is doubled.

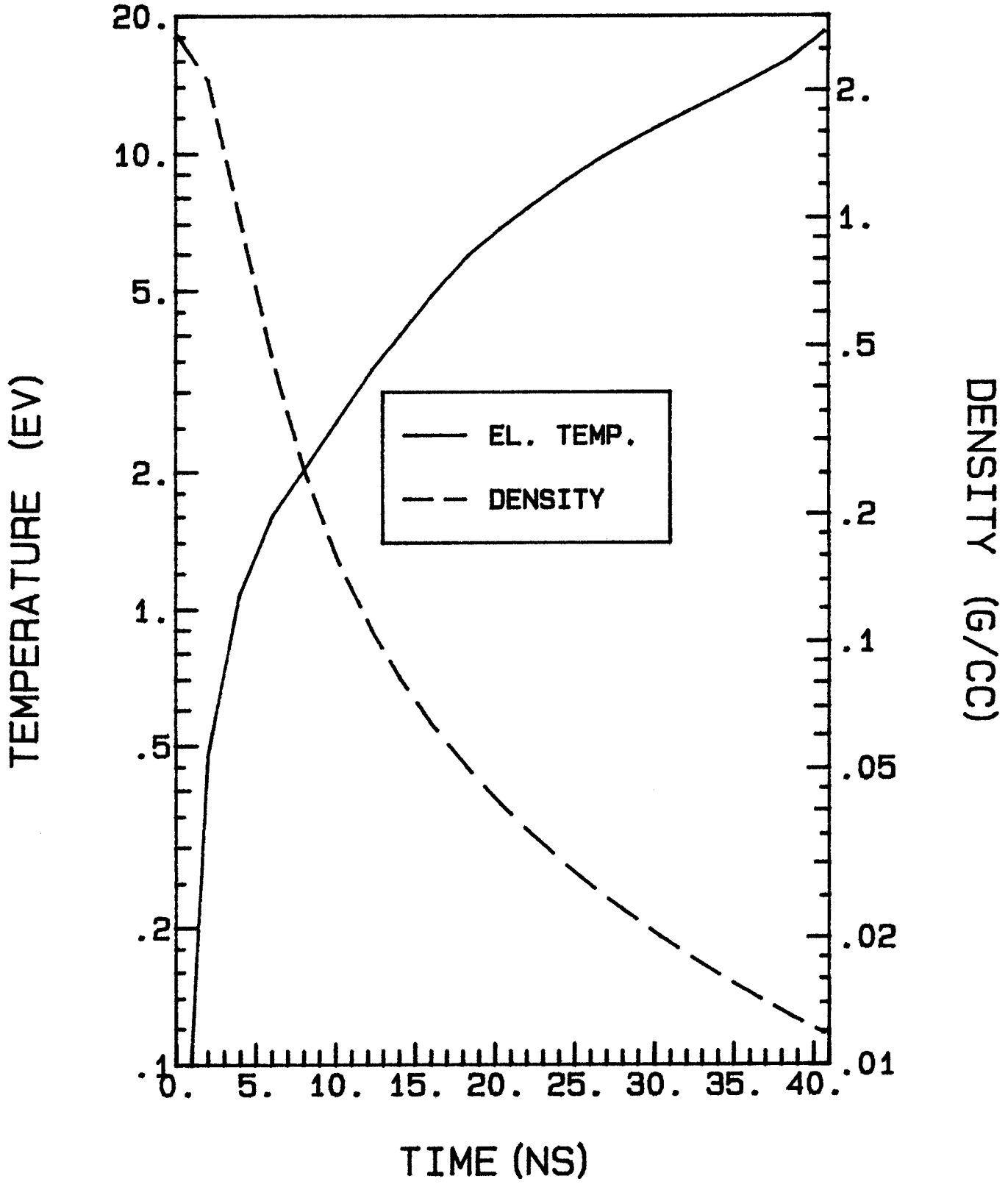

Fig. 24. Midplane Electron Temperature and Mass Density in a 7.5 μm Thick Aluminum Target versus Time. The species are the same as in Fig. 22, but the pulse has been compressed aand the diode voltage is doubled.

done for a 3 TW beam, where the maximum diode voltage was 1.5 MV, as in the earlier calculation. The energy partition and the midplane density and temperature are shown in Figs. 25 and 26, respectively. In this case radiation losses become more important at an earlier stage, and, in spite of a 7 fold higher energy coupling, the temperature rises to only about 60 eV.

VII. SUMMARY AND CONCLUSIONS

In this paper it has been shown that the computer codes MEDUSA-KA and PHD-IV with their recent modifications, are suitable to analyze energy deposition experiments. The results of calculations with these codes agree well with the results of Rogerson et al. for a 1 MeV 16 TW proton beam incident on a 15 μm aluminum slab. KALIF, with its present characteristics, is suitable to measure dE/dx in aluminum in the temperature range of 3 eV to 25 eV. An increase in power densities would extend the range towards higher temperature. At these temperatures, however, radiation cooling of the target becomes important. Thus an 8 fold increase in power density would extend the temperature range of the measurement only by a factor of 3 (i.e., to about 60 eV).

Acknowledgement

Support for this work has been provided by the Kernforschungszentrum Karlsruhe, through research agreement with Fusion Power Associates.

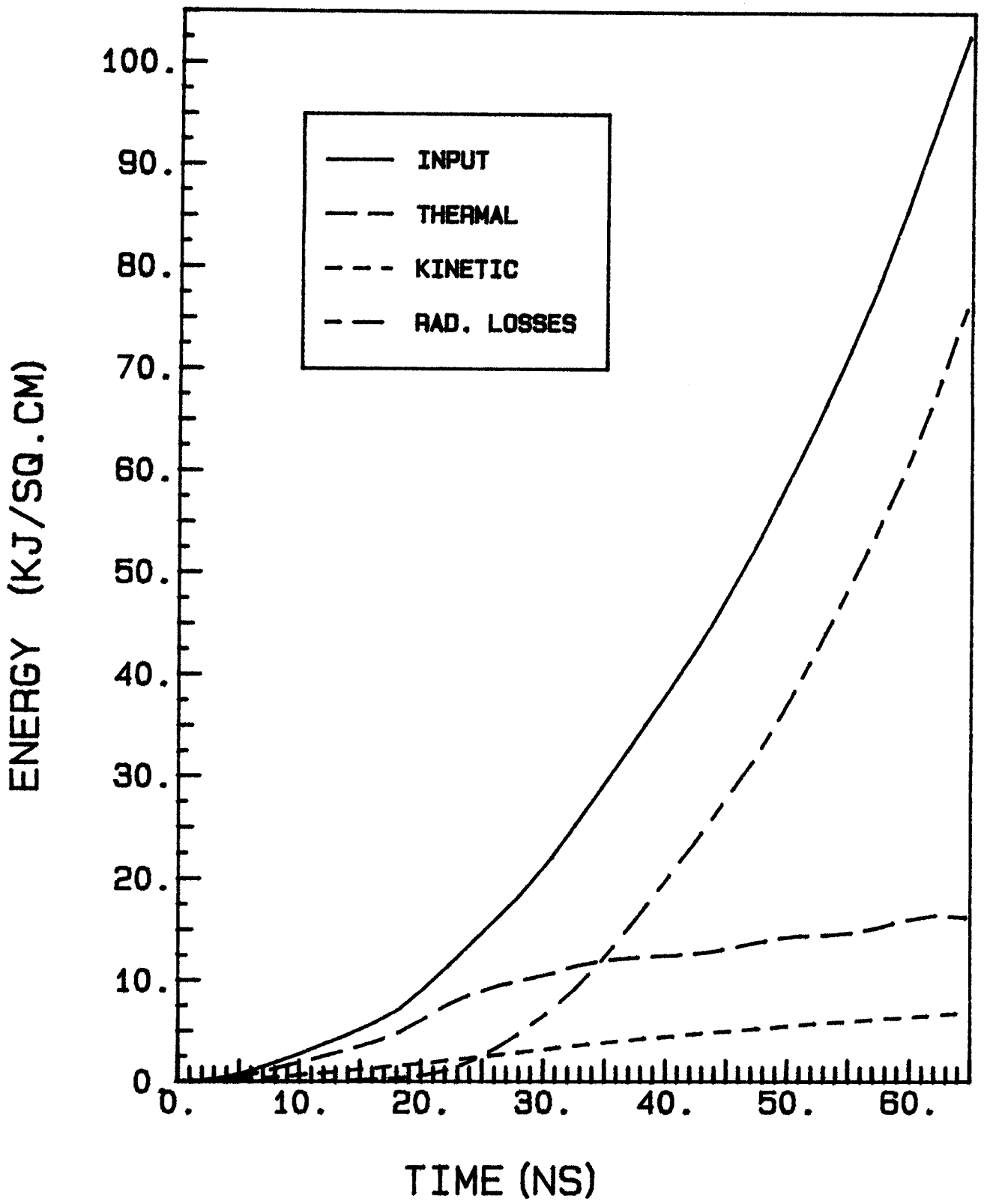

Fig. 25. Energy Partitioning between Thermal, Kinetic, and Radiation and the Total Input Energy in a 7.5 μm Thick Aluminum Target versus Time. The species and the diode voltages are the same as in Fig. 22, but the total power has been doubled to reach a maximum of 3 TW.

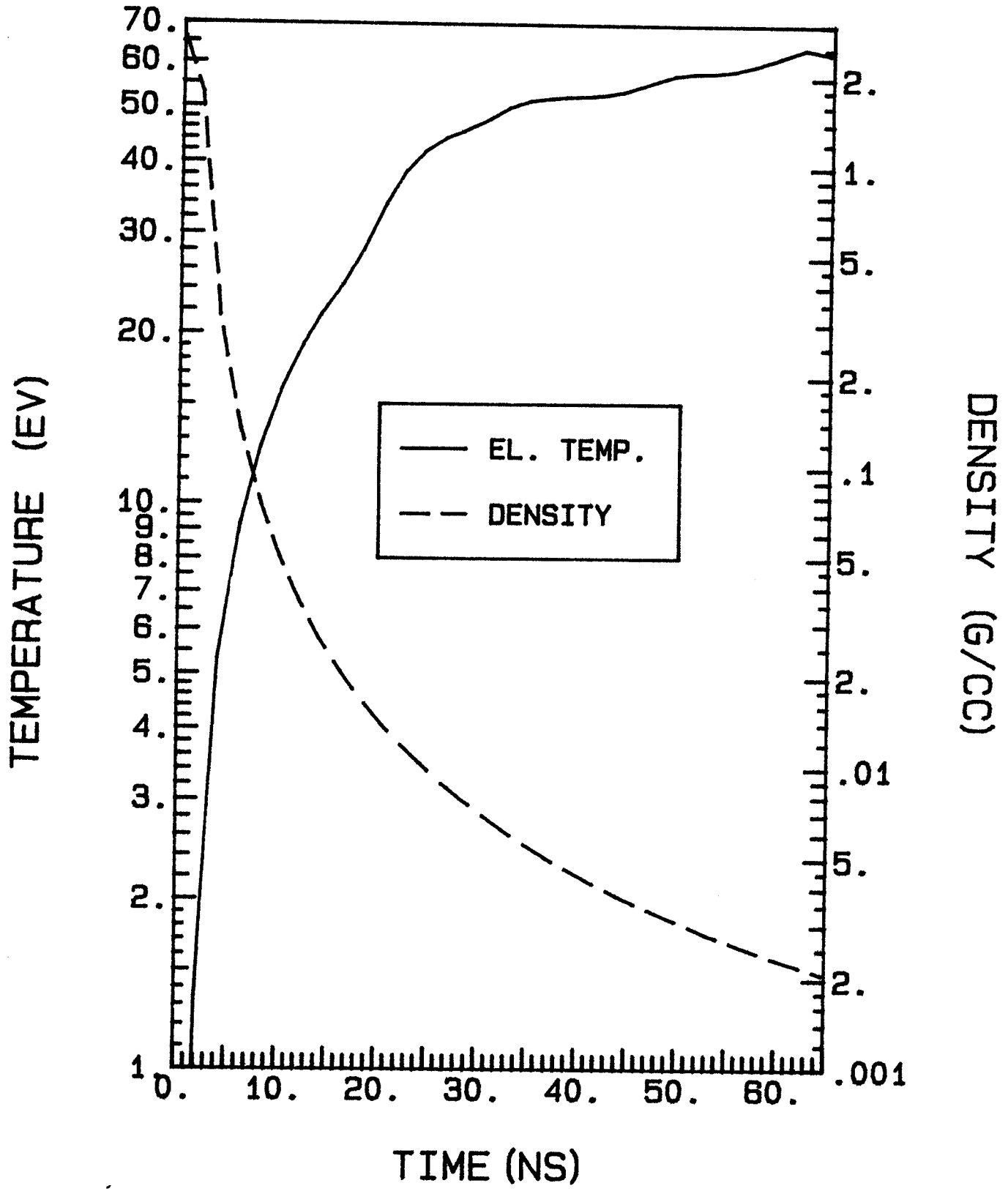

Fig. 26. Midplane Electron Temperature and Mass Density in a 7.5 μm Thick Aluminum Target versus Time. The species and the diode voltages are the same as in Fig. 22, but the total power has been doubled to reach a maximum of 3 TW.

REFERENCES

1. D. Mosher, G. Cooperstein, S.J. Stephanakis, S. Goldstein, D.J. Colombant and R. Lee, NRL Report 3658, (1977), Naval Research Lab.

2. A.V. Dobkin and I.V. Nemchivov, Sov. J. Plasma Phys. 8, 54 (1982).

3. Y.S. Sayasov, Helv. Phys. 57, 72 (1983).

4. R.G. Evans, Laser and Particle Beams 1, 231 (1983).

5. K.A. Long and N.A. Tahir, Phys. of Fluids 29, 275 (1986).

6. F.C. Young, D. Mosher, S.J. Stephanakis, S.A. Goldstein and T.A. Mehlhorn, Phys. Rev. Lett. 49, 549 (1982).

7. J.N. Olsen, T.A. Mehlhorn, J. Manechen and D.J. Johnson, J. Appl. Phys., (1985).

8. H. Bluhm, K. Boehnel, L. Buth, P. Hoppé, H.V. Karow, A. Klumpp, D. Rusch, T. Scherer, U. Schuelken and J. Singer, IEEE meeting, 1985.

9. J.E. Rogerson, R.W. Clark and J. Davis, Phys. Rev. A31, 3323 (1985).

10. J.P. Christiansen, D.E.T.F. Ashby and K.V. Roberts; Comp. Phys. Comm. 7, 271 (1974).

11. N.A. Tahir and K.A. Long; KfK 3454, Karlsruhe (1983).

12. B. Goel and W. Höbel, Plasma Physics and Controlled Nuclear Fusion Research, London, 12-19 September 1984, Nuclear Fusion Supplement 1985, Vol. 3, p. 345.

13. G.A. Moses, Nucl. Sci. Engr. 64, 49 (1977).

14. G.R. Magelssen and G.A. Moses, Nucl. Fus. 19, 301 (1979).

15. L. Spitzer, Jr., Physics of Fully Ionized Gases, 2nd Edition, John Wiley & Sons, New York, p. 125.

16. W.F. Huebner, A.L. Merts, N.H. Magee, Jr., and M.F. Argo, LA-6760-M, Los Alamos (1977).

17. B.I. Bennet, J.D. Johnson, G.I. Kerley and G.T. Road, LA-7130, Los Alamos (1978).

18. A.R. Bell, RL-80-91 Rutherford (1981).

19. D.A. Kirzhnits, Sov. Phys. JETP 8, 1081 (1959).

20. J.F. Ziegler, Stopping Cross Section for Energetic Ions in All Elements, Vol. 5, Pergamon Press, New York, 1980.

21. E. Nardi and Z. Zinamon, Phys. Rev. Lett. 49, 1251 (1982).

22. E. Nardi, E. Pelleg and Z. Zinamon, Phys. Fluids 21, 574 (1978); and Appl. Phys. Lett. 39, 46 (1981).

23. C. Deutsch, G. Maynard and H. Minoo, in GSI-82-8, p. 543, Darmstadt (1982).

24. T.A. Mehlhorn, J. Appl. Phys. 52, 6522 (1981).

25. T.A. Mehlhorn, J.M. Peek, E.J. McGuire, J.N. Olson, F.C. Young, J. De Physique, Colloque 44, C8-39 (1983).

26. E.J. McGuire, J.M. Peek and L.C. Pitchford, Phys. Rev. A26, 1318 (1982).

27. T.D. Beynon, Phil. Trans. Roy. Soc. London A300, 613 (1981).

28. W. Geiger, H. Hornberg and K.H. Schramm, Springer Tracts of Modern Physics 46, 1 (1968).

29. H.A. Bethe, Ann. d. Physik (Leipzig) 5, 325 (1930).

30. K.A. Long, N. Moritz and N.A. Tahir, KfK-3608, Karlsruhe (1983).

31. D. Duston, R.W. Clark, J. Davis, J.P. Apruzese, Phys. Rev. A21, 1441 (1983).